Supporting Information for

One-step selective synthesis of doubly and triply fused chiral boroloborole derivatives

Josina L. Bohlen,[a,b] Nele Wieprecht,[a,b] Merle Arrowsmith,[a,b] Alena Häfner,[a,b] Marco Neder,[a,b] Holger Braunschweig*[a,b]

[a] *Institute for Inorganic Chemistry, Julius-Maximilians-Universität Würzburg, Am Hubland, 97074 Würzburg, Germany.*
[b] *Institute for Sustainable Chemistry & Catalysis with Boron, Julius-Maximilians-Universität Würzburg, Am Hubland, 97074 Würzburg, Germany.*

Contents

Methods and materials

All manipulations were performed either under an atmosphere of dry argon or *in vacuo* using standard Schlenk line or glovebox techniques. Deuterated solvents were dried over molecular sieves and degassed by three freeze-pump-thaw cycles prior to use. All other solvents were distilled and degassed from appropriate drying agents. Both deuterated and non-deuterated solvents were stored under argon over activated 4 Å molecular sieves. Liquid-phase NMR spectra were acquired on a Bruker Avance Neo I 600 spectrometer (^{1}H: 600.2 MHz, ^{11}B: 192.6 MHz, ^{13}C: 150.9 MHz) at room temperature if not stated otherwise. Chemical shifts (δ) are reported in ppm and internally referenced to the carbon nuclei (^{13}C{^{1}H}) or residual protons (^{1}H) of the solvent. Heteronuclei NMR spectra are referenced to external standards (^{11}B: $BF_3{\cdot}OEt_2$). Resonances are given as singlet (s), doublet (d), triplet (t), septet (sept), multiplet (m), or broad (br). High-resolution mass spectrometry (HRMS) data were obtained from a Thermo Scientific Exactive Plus spectrometer. Unless stated otherwise, solvents and reagents were purchased from Sigma-Aldrich or Alfa Aesar.

1,2-bis(dichloroboryl)benzene (**1^{Bz}**),[1] 2,3-bis(dibromoboryl)naphthalene (**1^{Naph}**),[2] 2,3,4,5-tetraphenyl-1,1-dimethyl-1*H*-stannole (**2-Ph**),[3] 2,3,4,5-tetraethyl-1,1-dimethyl-1*H*-stannole (**2-Et**),[4] of 2,3-diphenyl-1-zirconaindene,[5] and I*i*Pr (1,3-di*iso*propylimidazol-2-ylidene),[6] were synthesized using literature procedures.

Synthetic procedures

Synthesis of 2-BzPh

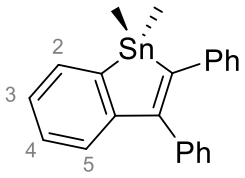

To a solution of 2,3-diphenyl-1-zirconaindene (7.25 g,15.24 mmol) in THF (50 mL) Me_2SnCl_2 was added. The reaction mixture was stirred overnight at 80 °C, prior to removal of the solvent *in vacuo*. The resulting solid residue was washed with *n*-pentane (150 mL), filtered over Celite, and the filtrate dried *in vacuo*. Any remaining Me_2SnCl_2 was removed by sublimation at 50 °C under high vacuum. The resulting colourless solid was recrystallized from *n*-hexane at –20 °C, affording pure **2-BzPh** (3.38 g, 8.37 mmol, 58%). **^{1}H NMR** (400 MHz, benzene-d_6): δ (ppm) = 7.60–7.47 (ddd with satellites, $^3J_{H\text{-}H}$ = 6.8 Hz, $^4J_{H\text{-}H}$ = 1.5 Hz, $^5J_{H\text{-}H}$ = 0.6 Hz, $^3J_{Sn\text{-}H}$ = 38.5 Hz, 1H, *H1*), 7.24 (ddd with satellites, $^3J_{H\text{-}H}$ = 7.7 Hz, $^4J_{H\text{-}H}$ = 1.3 Hz, $^5J_{H\text{-}H}$ = 0.6 Hz, $^4J_{Sn\text{-}H}$ = 11.5 Hz, 1H, *H5*), 7.22–7.16 (m overlapping with solvent resonance, 3H, CH_{Ar}), 7.08–7.14 (m, 5H, CH_{Ar}), 7.06–6.99 (m, 3H, CH_{Ar}), 6.89–6.85 (ddt, $^3J_{H\text{-}H}$ = 7.7, 7.0 Hz, $^4J_{H\text{-}H}$ = 1.5 Hz, 1H, *H*4), 0.37 (s with $^{117/119}$Sn satellites, $^2J_{Sn\text{-}H}$ = 59.0, 56.2 Hz, 6H, CH_3). These data are in agreement with those reported in the PhD Thesis of A. Y. Houghton, 2014.[7]

Synthesis of 3^{Bz}-Ph

To a solution of **2-Ph** (527 mg, 1.04 mmol) in benzene (10 mL) a solution of **1^{Bz}** (250 mg, 1.04 mmol) in benzene (5 mL) was added dropwise. The resulting dark violet reaction mixture was stirred over night at room temperature, whereby a slow colour change towards green occurred, prior to the removal of all volatile components *in vacuo*. The solid residue was extracted with pentane and the filtrate dried *in vacuo*. Washing of the resulting solid residue with cold pentane and drying *in vacuo* afforded **3^{Bz}-Ph** as a light green solid (430 mg, 0.819 mmol, 78%). Single crystals of **3^{Bz}-Ph** suitable for X-ray diffraction analysis were obtained by slow evaporation of a saturated benzene solution at 20 °C. **^{1}H NMR** (600 MHz, benzene-d_6): δ (ppm) = 7.83–7.81 (m, 1H, C2*H*), 7.68–7.66 (m, 1H, C5*H*), 7.24–7.22 (m, 5H, C4*H* + CH_{Ph}), 7.08–7.07 (m, 2H, CH_{Ph}), 7.06–7.03 (m, 3H, C3*H* + CH_{Ph}), 6.98–6.95 (m, 1H, CH_{Ph}), 6.86–6.79 (m, 5H, CH_{Ph}), 6.77–6.72 (m, 5H, CH_{Ph}), 6.67 (br s, 1H, CH_{Ph}). **^{11}B NMR** (193 MHz, benzene-d_6): δ (ppm) = 69.5 (br, fwhm ≈ 1550 Hz). **^{13}C{^{1}H,^{11}B} NMR** (151 MHz, benzene-d_6): δ (ppm) = 183.2 (C9), 164.2 (C6), 148.0 (C10), 145.2 (*i*-C_{Ph}), 142.1 (*i*-C_{Ph}), 139.7 (C1), 138.1 (*i*-C_{Ph}), 138.1 (*i*-C_{Ph}), 136.6 (*C*4H), 133.1 (*C*2H), 131.4 (*C*H$_{Ph}$), 131.3 (*C*H$_{Ph}$), 129.4 (*C*H$_{Ph}$), 129.1 (*C*5H), 128.5 (*C*H$_{Ph}$), 128.4 (*C*H$_{Ph}$), 128.1 (*C*H$_{Ph}$), 127.8 (*C*H$_{Ph}$), 127.8 (*C*H$_{Ph}$),

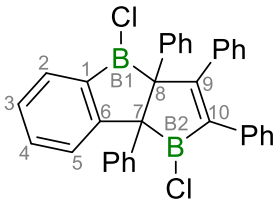

126.9 (*C*H$_{Ph}$), 126.6 (*C*H$_{Ph}$), 126.0 (*C*H$_{Ph}$), 77.8 (C8), 73.1 (C7). **HRMS LIFDI** (*m/z*) for [$C_{34}H_{24}B_2Cl_2$] = [M]: calcd. 524.1436; found 524.1426.

Synthesis of 3^{Bz}-Et

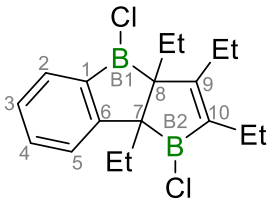

To a solution of **2-Et** (327 mg, 1.04 mmol) in benzene (7 mL) a solution of **1^{Bz}** (250 mg, 1.04 mmol) in benzene (3 mL) was added dropwise, upon which the reaction solution first turned red, then slowly discoloured at room temperature. The reaction mixture was stirred over night at room temperature prior to the removal of all volatile components *in vacuo*. Extraction of the residue with pentane and removal of the filtrate solvent *in vacuo* afforded **3^{Bz}-Et** as a light-red oily substance (314 mg, 0.944 mmol, 90%). Single crystals of **3^{Bz}-Et** suitable for X-ray diffraction analysis were obtained by slow evaporation of a saturated pentane solution at –30 °C. **^{1}H NMR** (600 MHz, benzene-d_6): δ (ppm) = δ_A 7.63 (1H, C2*H*), δ_B 6.93 (1H, C3*H*), δ_C 7.26 (1H, C4*H*), δ_D 7.57 (1H, C5*H*, ABCD spin system, $^5J_{AD}$ = 0.8 Hz, $^4J_{AC}$ = 1.3 Hz, $^3J_{AB}$ = 7.3 Hz, $^3J_{DC}$ = 7.9 Hz, $^4J_{DB}$ = 0.9 Hz, $^3J_{CB}$ = 7.3 Hz), 2.60 (dq, ^3J = 7.7 Hz, ^2J = 12.5 Hz, 1H, C9-C*H*$_{2\text{-Et}}$), 2.42 (dq, ^3J = 7.7 Hz, ^2J = 12.5 Hz, 1H, C9-C*H*$_{2\text{-Et}}$), 2.26 (dq, ^3J = 7.5 Hz, ^2J = 14.1 Hz, 1H, C7-C*H*$_{2\text{-Et}}$), 2.13 (dq, ^3J = 7.6 Hz, ^2J = 14.0 Hz, 1H, C8-C*H*$_{2\text{-Et}}$), 2.10–2.03 (m, 1H each of C7-C*H*$_{2\text{-Et}}$ and C10-C*H*$_{2\text{-Et}}$), 2.01–1.94 (m, 1H each of C8-C*H*$_{2\text{-Et}}$ and C10-C*H*$_{2\text{-Et}}$), 0.93 (t, ^3J = 7.6 Hz, 3H, C10-C*H*$_{3\text{-Et}}$), 0.90 (t, ^3J = 7.7 Hz, 3H, C9-C*H*$_{3\text{-Et}}$), 0.77 (t, ^3J = 7.5 Hz, 3H, C7-C*H*$_{3\text{-Et}}$), 0.65 (t, ^3J = 7.5 Hz, 3H, C8-C*H*$_{3\text{-Et}}$). **^{11}B NMR** (193 MHz, benzene-d_6): δ (ppm) = 67.9 (br, fwhm ≈ 520 Hz). **^{13}C{^{1}H,^{11}B} NMR** (151 MHz, benzene-d_6): δ (ppm) = 188.8 (C9), 165.1 (C6), 144.2 (C10), 138.0 (C1), 135.9 (*C*4H), 132.5 (*C*2H), 126.7 (*C*3H), 125.1 (*C*5H), 66.6 (C8), 60.2 (C7), 25.5 (C7-*C*H$_{2\text{-Et}}$), 23.5 (C9-*C*H$_{2\text{-Et}}$), 22.8 (C8-*C*H$_{2\text{-Et}}$), 20.4 (C10-*C*H$_{2\text{-Et}}$), 14.8 (C10-*C*H$_{3\text{-Et}}$), 14.1 (C9-*C*H$_{3\text{-Et}}$), 13.2 (C7-*C*H$_{3\text{-Et}}$), 13.2 (C8-*C*H$_{3\text{-Et}}$). **HRMS LIFDI** (*m/z*) for [$C_{18}H_{24}B_2Cl_2$] = [M]: calcd. 332.1436; found 332.1433.

Synthesis of 3^{Naph}-Ph

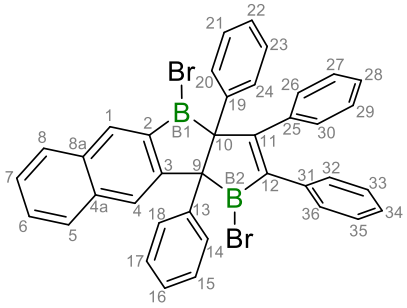

To a solution of **2-Ph** (75.7 mg, 0.150 mmol) in benzene (2.5 mL) a solution of **1^{Naph}** (70.0 mg, 0.150 mmol) in benzene (2.5 mL) was added dropwise. The resulting dark green reaction solution was stirred overnight at room temperature. Subsequently, the solvent was removed *in vacuo* and the residue extracted with pentane. The solution was cooled, resulting in precipitation of a green solid.

Filtration and drying *in vacuo* afforded **3^{Naph}-Ph** as a light green solid (27.0 mg, 0.041 mmol, 27%). Single crystals of **3^{Naph}-Ph** suitable for X-ray diffraction analysis were obtained by slow evaporation of a saturated pentane solution at 20 °C. **^{1}H NMR** (500 MHz, benzene-d_6): δ (ppm) = 8.55 (s, 1H, C1*H*), 8.30 (s, 1H C4*H*); δ_A 7.62 (1H, C8*H*), δ_B 7.10 (1H, C7*H*), δ_C 7.16 (1H, C6*H*), δ_D 7.43 (1H, C5*H*) (ABCD spin system, $^{5}J_{AD}$ = 0.6 Hz, $^{4}J_{AC}$ = 1.2 Hz, $^{3}J_{AB}$ = 8.3 Hz, $^{3}J_{DC}$ = 8.3 Hz, $^{4}J_{DB}$ = 1.2 Hz, $^{3}J_{CB}$ = 6.9 Hz); 7.30–7.28 (m, 2H, *o*-C26/30*H*), 7.26–7.24 (m, 2H, *o*-C32/36*H*), 7.21–7.20 (m, 2H, *o*-C20/24*H*), 7.05–7.01 (m, 2H, *m*-C33/35*H*), 6.97–6.94 (m, 1H, *p*-C34*H*), 6.93–6.87 (m, 2H, *m*-C21/23*H*), 6.89–6.86 (m, 1H, *p*-C22*H*) 6.85–6.82 (m, 1H, *p*-C28*H*), 6.80–6.73 (m, 7H, *o*-C14/18*H*, *m*-C15/18*H*, *p*-C16*H*, *m*-C27/29*H*). **^{11}B NMR** (193 MHz, benzene-d_6): δ (ppm) = 71.9 (br, fwhm ≈ 2150 Hz). **^{13}C{^{1}H,^{11}B} NMR** (126 MHz, benzene-d_6): δ (ppm) = 182.8 (C11), 154.7 (C3), 151.2 (C12), 146.1 (*i*-C13), 142.3 (*i*-C19), 140.7 (C2), 138.7 (C4a), 138.3 (*i*-C25), 138.2 (*i*-C31), 137.8 (*C*1H), 133.4 (C8a), 131.9 (*o*-*C*14/18H), 131.5 (*o*-*C*20/24H), 131.3 (*o*-*C*26/30H), 130.6 (*C*8H), 130.4 (*o*-*C*32/36H), 129.6 (*C*6H), 129.5 (*p*-*C*28H), 128.7 (*C*5H), 128.5 (*m*-*C*33/35H), 128.4 (*C*4H), 128.1 (*m*-*C*21/23H), 127.9 (*m*-*C*27/29H), 127.7 (*m*-*C*15/17H), 126.9 (*p*-*C*34H), 126.7 (*p*-*C*22H) 126.4 (*C*7H), 126.0 (*p*-*C*16H), 81.2 (C10), 74.7 (C9). **HRMS LIFDI** (*m/z*) for [$C_{38}H_{28}B_2O_2$] = [M – 2Br + 2OH]: calcd. 538.2270; found 538.2264. *Note: due to the sensitivity of the compound, only the hydrolysis product was observed*.

Synthesis of 3^{Naph}-Et

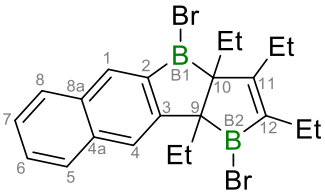

To a solution of **2-Et** (67.0 mg, 0.214 mmol) in benzene (2.0 mL) a solution of **1^{Naph}** (100 mg, 0.214 mmol) in benzene (3 mL) was added dropwise, upon which the reaction solution first turned dark violet and then discoloured at room temperature. The resulting yellow mixture was stirred over night at room temperature prior to solvent removal *in vacuo* and extraction of the residue with cold pentane. Filtration and drying *in vacuo* afforded **3^{Naph}-Ph** as a viscous yellow oil (60.5 mg, 0.128 mmol, 60%). **^{1}H NMR** (600 MHz, benzene-d_6): δ (ppm) = 8.29 (s, 1H, C1*H*), 8.05 (s, 1H, C4*H*); δ_A 7.55 (1H, C8*H*), δ_B 7.07 (1H, C7*H*), δ_C 7.21 (1H, C6*H*), δ_D 7.62 (1H, C5*H*) (ABCD spin system, $^{5}J_{AD}$ = 0.61 Hz, $^{3}J_{DC}$ = 8.4 Hz, $^{4}J_{AC}$ = 1.2 Hz, $^{4}J_{DB}$ = 1.2 Hz, $^{3}J_{AB}$ = 8.3 Hz, $^{3}J_{CB}$ = 6.8 Hz), 2.69 (dq, ^{3}J = 7.6 Hz, ^{2}J = 12.4 Hz, 1H, C11-C$H_{2\text{-Et}}$), 2.48 (dq, ^{3}J = 7.7 Hz, ^{2}J = 12.5 Hz, 1H, C11-C$H_{2\text{-Et}}$), 2.41 (dq, ^{3}J = 7.2 Hz, ^{2}J = 14.9 Hz, 1H, C9-C$H_{2\text{-Et}}$), 2.23–2.17 (m, 2H, 1H each of C9-C$H_{2\text{-Et}}$ and C15-C$H_{2\text{-Et}}$), 2.16–2.12 (m, 1H, C12-C$H_{2\text{-Et}}$), 2.12–2.04 (m, 2H, 1H each of C10-C$H_{2\text{-Et}}$ and C12-C$H_{2\text{-Et}}$),

0.96 (t, ^{3}J = 7.53 Hz, 3H, C12-C$H_{3\text{-Et}}$), 0.93 (t, ^{3}J = 7.56 Hz, 3H, C11-C$H_{3\text{-Et}}$), 0.78 (t, ^{3}J = 7.44 Hz 3H, C9-C$H_{3\text{-Et}}$), 0.64 (t, ^{3}J = 7.49 Hz, 3H, C10-C$H_{3\text{-Et}}$). **^{11}B NMR** (193 MHz, benzene-d_6): δ (ppm) = 70.4 (br, fwhm ≈ 1040 Hz). **^{13}C{^{1}H,^{11}B} NMR** (151 MHz, benzene-d_6): δ (ppm) = 189.1 (C11), 156.5 (C3), 147.1 (C12), 139.4 (C2), 138.6 (C4a), 136.4 (C1), 133.0 (C8a), 130.5 (C8), 129.2 (C6), 128.4 (C5), 125.6 (C7), 123.2 (C4), 69.9 (C10), 61.7 (C9), 26.5 (C9-CH$_{2\text{-Et}}$), 24.0 (C11-CH$_{2\text{-Et}}$), 23.2 (C10-CH$_{2\text{-Et}}$), 20.9 (C12-CH$_{2\text{-Et}}$), 15.0 (C12-CH$_{3\text{-Et}}$), 14.1 (C11-CH$_{3\text{-Et}}$), 13.2 (C9-CH$_{3\text{-Et}}$), 12.9 C10-CH$_{3\text{-Et}}$). **HRMS LIFDI** (*m/z*) for [$C_{22}H_{27}BBr_2$]$^{+}$ = [M + H]$^{+}$: calcd. 472.0561; found 472.0560.

Synthesis of 4^{Bz}-Et

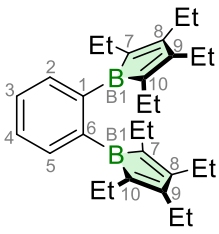

To a solution of **2-Et** (26.1 mg, 0.085 mmol) in toluene (0.25 mL) a solution of **1^{Bz}** (10.0 mg, 0.042 mmol) in toluene (0.25 mL) was added dropwise at room temperature, upon which the reaction mixture turned dark purple. The solution was immediately frozen using liquid nitrogen and thawed right before NMR-spectroscopic analysis at –40 °C. The NMR sample temperature was increased stepwise until full consumption of **2-Et** was observed at 25 °C. Due to its instability in solution and decomposition upon solvent removal **4^{Bz}-Et** could not be isolated and was only characterised *in situ*. **^{1}H NMR** (500 MHz, toluene-d_8): δ (ppm) = 7.67 (2H, AA'XX' spin system, td, $^{3}J_{AX/A'X'/XX'}$ = 7.5 Hz, $^{4}J_{A'X/AX'}$ = 1.3 Hz, C3H + C4H), 7.25 (2H, AA'XX' spin system, ddd, $^{3}J_{AX/A'X'}$ = 7.5 Hz, $^{4}J_{A'X/AX'}$ = 1.3 Hz, $^{5}J_{AA'}$ = 0.8 Hz, C2H + C5H), 2.27 (q, ^{3}J = 7.5 Hz, 8H, C7-C$H_{2\text{-Et}}$ and C10-C$H_{2\text{-Et}}$), 2.09 (q, ^{3}J = 7.5 Hz, 8H, C8-C$H_{2\text{-Et}}$ and C9-C$H_{2\text{-Et}}$), 1.00 (t, ^{3}J = 7.5 Hz, 12H, C8-C$H_{3\text{-Et}}$ and C9-C$H_{3\text{-Et}}$), 0.87 (t, ^{3}J = 7.5 Hz, 12H, C7-C$H_{3\text{-Et}}$ and C10-C$H_{3\text{-Et}}$). **^{11}B NMR** (161 MHz, toluene-d_8): δ (ppm) = 69.4 (br, fwhm ≈ 1470 Hz). **^{13}C{^{1}H} NMR** (125.8 MHz, toluene-d_8): δ (ppm) = 163.9 (C8, C9), 145.9 (C1, C6), 138.3 (C7, C10), 131.6 (C3, C4), 129,6 (C2, C5), 21.1 (C7-CH$_{2\text{-Et}}$ and C10-CH$_{2\text{-Et}}$), 21.1 (C8-CH$_{2\text{-Et}}$ and C9-CH$_{2\text{-Et}}$), 16.0 (C7-CH$_{3\text{-Et}}$ and C10-CH$_{3\text{-Et}}$), 0.87 (C8-CH$_{3\text{-Et}}$ and C9-CH$_{3\text{-Et}}$). *Note: the compound proved too unstable for further characterisation by HRMS or elemental analysis.*

Synthesis of 4^{Bz}-BzPh

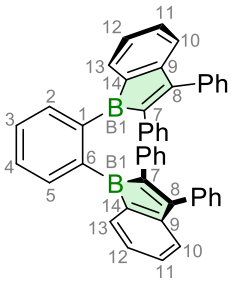

To a solution of **2-BzPh** (50.0 mg, 0.124 mmol, 2.00 equiv) in benzene (3.0 mL) $\mathbf{1^{Bz}}$ (14.9 mg, 62.0 µmol, 1.00 equiv) was added and the mixture was stirred for 5 min, during which it turned from colorless to dark red. The solution was stirred for 16 h. All volatiles were removed *in vacuo* and the side product dimethyltin dibromide was removed from the product by sublimation at 60 °C. The remaining solid was washed with *n*-pentane (4 × 0.5 mL) and dried again, yielding **4^{Bz}-BzPh** as a red solid (23.0 mg, 37.9 µmol, 61%). Single crystals suitable for X-ray diffraction analysis were obtained by slow evaporation of a saturated benzene solution at room temperature. **^{1}H NMR** (600 MHz, benzene-d_6): δ (ppm) = 7.77 (2H, AA'XX' spin system, ddd, $^{3}J_{AX/A'X'}$ = 7.4 Hz, $^{3}J_{XX'}$ = 7.5 Hz, $^{4}J_{AX'/A'X}$ = 1.5 Hz, C3*H* + C4*H*), 7.33 (2H, AA'XX' spin system, ddd, $^{3}J_{AX/A'X'}$ = 7.4 Hz, $^{4}J_{AX'/A'X}$ = 1.5 Hz, $^{5}J_{AA'}$ = 0.5 Hz C2*H* + C5*H*) 7.30–7.25 (m, 2H, C13*H*), 7.11–7.08 (m, 4H, CH_{Ph}), 7.04–7.00 (m, 2H, CH_{Ph}), 6.99–6.96 (m, 1H, CH_{Ph}), 6.86–6.77 (m, 12H, C10*H* + C12*H* + CH_{Ph}), 6.69–6.65 (m, 2H, CH_{Ph}), 6.64–6.61 (m, 2H, C11*H*), **^{11}B NMR** (193 MHz, benzene-d_6): δ (ppm) = 66.8 (br s, fwhm ≈ 2680 Hz), **^{13}C{^{1}H} NMR** (151 MHz, benzene-d_6): δ (ppm) δ = 164.3 (*C*8), 155.5 (*C*9), 147.0 (C7), 145.5 (C1, C6), 140.6 (C14), 137.9 (*i*-C_{Ph}), 136.5 (*i*-C_{Ph}), 134.1 (C3, C4), 133.5 (C13), 132.4 (C12), 130.9 (*C*H$_{Ph}$), 130.1 (C2, C5), 128.9 (*C*H$_{Ph}$), 128.5 (*C*H$_{Ph}$), 128.4 (*C*H$_{Ph}$), 128.1 (*C*H$_{Ph}$), 127.9 (*C*H$_{Ph}$), 127.6 (C10), 125.9 (*C*H$_{Ph}$), 121.4 (C11). **Elemental analysis** calcd. for $C_{46}H_{38}B_2$ [612.43 g/mol]: C 90.22, H 6.25; found: C 89.86, H 5.67.

Synthesis of 3^{Bz}-BzPh

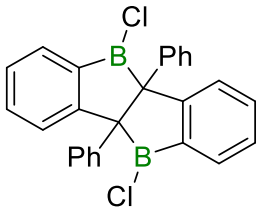

To a solution of $\mathbf{1^{Bz}}$ (30.0 mg, 125 µmol, 1.00 equiv.) in C_6D_6 **2-BzPh** (50.5 mg, 125 µmol, 1.00 equiv.) was added, upon which the solution immediately turned deep red. The mixture was first heated at 60 °C overnight and then at 80 °C for another two days, while regularly monitoring the reaction by ^{1}H and ^{11}B NMR spectroscopy. Once no more change was observable in the spectra, the solvent was removed *in vacuo* and the residue dried under high vacuum at 60 °C for 4 hours. The resulting solid residue was extracted with pentane (3 × 1 mL) and slow evaporation at –40 °C yielded a handful of yellow crystals of **3^{Bz}-BzPh**. Although reproducible, the amount of material collected was always insufficient for full NMR-spectroscopic characterisation. **^{11}B NMR** (129 MHz, benzene-d_6): δ (ppm) = 66.0 (br s, fwhm ≈ 2196 Hz).

Synthesis of 5/6^{Bz}-Ph

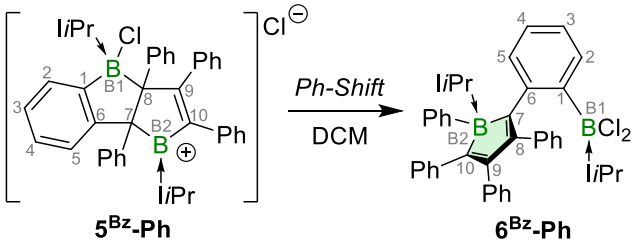

5^{Bz}-Ph **6^{Bz}-Ph**

To a solution of **3^{Bz}-Ph** (30.0 mg, 0.063 mmol) in benzene (2.5 mL) a solution of 1,3-di*iso*propyl-imidazol-2-ylidene (18.0 mg, 0.126 mmol) in benzene (2.5 mL) was added dropwise, resulting in the precipitation of a dark oily solid. The reaction mixture was left to stand at room temperature overnight, after which the benzene solution was discarded, and the remaining solid washed with benzene and redissolved in dichloromethane. Removal of the solvent afforded **5^{Bz}-Ph** a dark orange solid (33.0 mg, 39.8 µmol, 63%). *Note: **5^{Bz}-Ph** is only soluble in chlorinated solvents, in which it partly undergoes rearrangement to **6^{Bz}-Ph**, as determined by X-ray crystallographic analysis. NMR data of **5^{Bz}-Ph** was collected in tetrachloroethane-d_2, in which this reaction proved much slower than in dichloromethane-d_2. The increasing amount of **6^{Bz}-Ph** formed during data collection precludes the precise assignment of NMR resonances.* NMR data for **5^{Bz}-Ph**: **^{1}H NMR** (600 MHz, tetrachloroethane-d_2): δ (ppm) = 8.28 (br s, 1H, C*H*$_{Ph}$), 7.40-7.39 (m, 2H, C*H*$_{Ph}$), 7.34-7.30 (m, 4H, C*H*$_{Ph}$), 7.25-7.14 (m, 8H, C*H*$_{Ph}$), 6.97-6.88 (m, 5H, C*H*$_{Ph}$), 6.75 (m, 1H, C*H*$_{Ph}$), 6.62-6.61 (m, 2H, C*H*$_{Ph}$), 6.58-6.55 (m, 1H, C*H*$_{Ph}$), 6.45-6.43 (m, 4H, C*H*$_{Ph}$), 5.41 (br s, 1H, NHC$_{B2}$-NC*H*), 3.60 (br s, 1H, NHC$_{B2}$-NC*H*), 3.39 (sept, ^3J = 6.4 Hz, 1H, NHC$_{B1}$-NC*H*$_{iPr}$), 3.28 (sept, ^3J = 6.6 Hz, 1H, NHC$_{B1}$-NC*H*$_{iPr}$), 1.51 (br s, 3H, NHC$_{B1}$-C*H*$_{3\text{-}iPr}$), 1.10 (br s, 3H, NHC$_{B2}$-C*H*$_{3\text{-}iPr}$), 0.88 (d, ^3J = 6.3 Hz, 3H, NHC$_{B1}$-C*H*$_{3\text{-}iPr}$), 0.75 (d, ^3J = 6.4 Hz, 3H, NHC$_{B1}$-C*H*$_{3\text{-}iPr}$), 0.68 (br s, 3H, NHC$_{B2}$-C*H*$_{3\text{-}iPr}$), 0.65 (d, ^3J = 6.5 Hz, 3H, NHC$_{B2}$-C*H*$_{3\text{-}iPr}$), 0.58 (d, ^3J = 6.5 Hz, 3H, NHC$_{B1}$-C*H*$_{3\text{-}iPr}$), 0.31 (br s, 3H, NHC$_{B2}$-C*H*$_{3\text{-}iPr}$). **^{11}B NMR** (193 MHz, tetrachloroethane-d_2): δ (ppm) = 64.9 (very broad, B2, fwhm ≈ 5050 Hz), 3.5 (s, B1). **^{13}C{^{1}H,^{11}B} NMR** (151 MHz, tetrachloroethane-d_2): δ (ppm) = 202.8 (C9), 158.4 (C$_{carbene}$), 153.0 (*C*$_q$), 151.45 (C1), 147.1 (*C*$_q$), 143.3 (*C*$_q$), 142.7 (*C*$_q$), 141.0 (*C*$_q$), 139.3 (*C*$_q$), 138.2 (*C*$_q$), 134.6 (*C*H$_{Ph}$), 130.6 (*C*H$_{Ph}$), 129.8 (*C*H$_{Ph}$), 128.9 (*C*H$_{Ph}$), 128.8 (*C*H$_{Ph}$), 128.5 (*C*H$_{Ph}$), 128.3 (*C*H$_{Ph}$), 128.0 (*C*H$_{Ph}$), 127.5 (*C*H$_{Ph}$), 126.9 (*C*H$_{Ph}$), 126.5 (*C*H$_{Ph}$), 126.5 (*C*H$_{Ph}$), 125.7 (*C*H$_{Ph}$), 124.1 (*C*H$_{Ph}$), 121.0 (N*C*H), 120.5 (N*C*H), 118.9 (N*C*H), 118.7 (N*C*H), 82.3 (C8), 77.0 (C7), 53.6 (*C*H$_{iPr}$), 52.8 (*C*H$_{iPr}$), 51.5 (br, *C*H$_{iPr}$), 51.0 (br, *C*H$_{iPr}$), 25.0 (*C*H$_{3\text{-}iPr}$), 24.9 (br, *C*H$_{3\text{-}iPr}$), 24.4 (br, *C*H$_{3\text{-}iPr}$), 23.6 (*C*H$_{3\text{-}iPr}$), 23.5 (*C*H$_{3\text{-}iPr}$), 23.1 (*C*H$_{3\text{-}iPr}$). NMR data for **6^{Bz}-Ph**: **^{1}H NMR** (600 MHz, dichloromethane-d_2): δ (ppm) = 8.20 (br s, 1H, C*H*$_{Ar}$), 7.80 (m, 1H, C*H*$_{Ar}$), 7.36-7.25 (m, 2H, C*H*$_{Ar}$), 7.24 (m, 1H, C*H*$_{Ar}$), 7.19-7.15 (m, 2H, C*H*$_{Ar}$), 7.13-7.10 (m, 2H, C*H*$_{Ar}$), 7.03-7.00 (m, 2H, C*H*$_{Ar}$), 7.00 (s, 2H, NHC$_{B1}$-NC*H*), 6.99-6.96 (m, 2H, C*H*$_{Ar}$), 6.94-6.90 (m,

1H, CH_{Ar}), 6.90-6.86 (m, 1H, CH_{Ar}), 6.84-6.79 (m, 2H, CH_{Ar}), 6.79-6.74 (m, 1H, CH_{Ar}), 6.74-6.70 (m, 2H, CH_{Ar}), 6.68-6.62 (m, 2H, CH_{Ar}), 6.55-6.50 (m, 2H, CH_{Ar}), 6.41-6.36 (m, 1H, CH_{Ar}), 6.03-5.97 (m, 1H, CH_{Ar}), 5.60 (sept, ^3J = 5.9 Hz, 1H, NHC$_{B2}$-C$H_{i\text{Pr}}$), 5.05 (br, 2H, NHC$_{B1}$-C$H_{i\text{Pr}}$), 4.48 (sept, ^3J = 5.8 Hz, 1H, NHC$_{B2}$-C$H_{i\text{Pr}}$), 1.70 (d, ^3J = 6.1 Hz, 3H, NHC$_{B2}$-C$H_{3\text{-}i\text{Pr}}$), 1.19 (d, ^3J = 5.9 Hz, 3H, NHC$_{B2}$-C$H_{3\text{-}i\text{Pr}}$), 1.15-1.10 (m, 6H, NHC$_{B1}$-C$H_{3\text{-}i\text{Pr}}$), 0.93 (br s, 6H, NHC$_{B1}$-C$H_{3\text{-}i\text{Pr}}$), 0.77 (d, ^3J = 5.9 Hz, 3H, NHC$_{B2}$-C$H_{3\text{-}i\text{Pr}}$), 0.20 (d, ^3J = 5.8 Hz, 3H, NHC$_{B2}$-C$H_{3\text{-}i\text{Pr}}$). **^{11}B NMR** (193 MHz, dichloromethane-d_2): δ (ppm) = 2.4 (br, fwhm ≈ 420 Hz, B2), –5.6 (s, fwhm ≈ 40 Hz, B1). **^{13}C{^{1}H,^{11}B} NMR** (151 MHz, dichloromethane-d_2): δ (ppm) = 165.2 (C7), 160.4 (BC_q), 159.5 (BC_q), 158.9 (BC_q), 154.2 (BC_q), 152.0 (C_q), 150.0 (C_q), 148.8 (C_q), 145.9 (C_q), 144.2 (C_q), 144.1 (C_q), 142.0 (C_q), 133.3 (CH$_{Ar}$), 132.9 (CH$_{Ar}$), 130.9 (CH$_{Ar}$), 130.2 (CH$_{Ar}$), 126.4 (CH$_{Ar}$), 126.2 (CH$_{Ar}$), 125.2 (CH$_{Ar}$), 124.7 (CH$_{Ar}$), 124.1 (CH$_{Ar}$), 123.9 (CH$_{Ar}$), 123.2 (CH$_{Ar}$), 123.2 (CH$_{Ar}$), 117.4 (NHC$_{B1}$-NCH), 52.0 (NHC$_{B2}$-CH$_{i\text{Pr}}$), 50.8 (NHC$_{B2}$-CH$_{i\text{Pr}}$), 50.5 (NHC$_{B1}$-CH$_{i\text{Pr}}$), 25.3 (NHC$_{B2}$-CH$_{3\text{-}i\text{Pr}}$), 24.3 (NHC$_{B2}$-CH$_{3\text{-}i\text{Pr}}$), 23.8 (NHC$_{B1}$-CH$_{3\text{-}i\text{Pr}}$), 23.8 (NHC$_{B2}$-CH$_{3\text{-}i\text{Pr}}$), 23.4 (NHC$_{B2}$-CH$_{3\text{-}i\text{Pr}}$), 22.7 (NHC$_{B1}$-CH$_{3\text{-}i\text{Pr}}$). **HRMS LIFDI** (*m/z*) for [$C_{52}H_{56}B_2Cl_2N_4$] = [M]: calcd. 828.4063; found 828.4045.

Synthesis of 5^{Bz}-Et

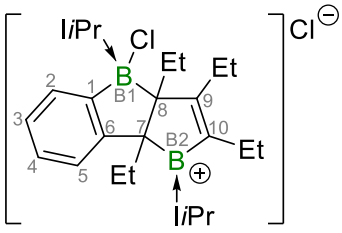

To a solution of **3^{Bz}-Et** (40.0 mg, 0.120 mmol) in benzene (2.5 mL) a solution of 1,3-di*iso*propylimidazol-2-ylidene (36.6 mg, 0.240 mmol) in benzene (2.5 mL) was added dropwise, resulting in the precipitation of a dark oily solid. The reaction mixture was left to stand at room temperature for 30 min, after which the benzene solution was discarded, and the remaining solid washed with benzene and redissolved in dichloromethane. Removal of the solvent afforded **5^{Bz}-Et** as a yellow-green solid (60.5 mg, 0.101 mmol, 84%). **^{1}H NMR** (600 MHz, dichloromethane-d_2): δ (ppm) = 8.20 (d, ^3J = 2.0 Hz, 1H, NCH), 7.52 (d, ^3J = 2.0 Hz, 1H, NCH), 7.47 (d, ^3J = 2.1 Hz, 1H, NCH), 7.38 (d, ^3J = 2.1 Hz, 1H, NCH), 7.07–7.02 (m, 3H, CH_{Bn}), 6.49–6.48 (m, 1H, CH_{Bn}), 6.05 (sept, ^3J = 6.6 Hz, 1H, NC$H_{i\text{Pr}}$), 4.26 (sept, ^3J = 6.7 Hz, 1H, NC$H_{i\text{Pr}}$), 3.96 (sept, ^3J = 6.5 Hz, 1H, NC$H_{i\text{Pr}}$), 3.24 (sept, ^3J = 6.5 Hz, 1H, NC$H_{i\text{Pr}}$), 2.76 (dq, ^3J = 7.3 Hz, ^2J = 15.4 Hz, 1H, C9-C$H_{2\text{-}Et}$), 2.56 (dq, ^3J = 7.3 Hz, ^2J = 15.0 Hz, 1H, C9-C$H_{2\text{-}Et}$), 2.31 (dq, ^3J = 7.3 Hz, ^2J = 15.0 Hz, 1H, C10-C$H_{2\text{-}Et}$), 2.12–1.97 (m, 3H, 1H of C9-C$H_{2\text{-}Et}$ and 2H of C7-C$H_{2\text{-}Et}$), 1.76 (d, ^3J = 6.5 Hz, 3H, C$H_{3\text{-}i\text{Pr}}$), 1.73–1.68 (m, 1H, C8-C$H_{2\text{-}Et}$), 1.64 (d, ^3J = 6.6 Hz, 3H, C$H_{3\text{-}i\text{Pr}}$), 1.55 (d, ^3J = 6.8 Hz, 3H, C$H_{3\text{-}i\text{Pr}}$), 1.52 (d, ^3J = 6.4 Hz, 3H, C$H_{3\text{-}i\text{Pr}}$), 1.53–1.50 (m, 1H, C8-C$H_{2\text{-}Et}$), 1.39

(t, ^3J = 7.6 Hz, 3H, C9-C$H_{3\text{-Et}}$), 1.22 (d, ^3J = 6.6 Hz, 3H, C$H_{3\text{-}i\text{Pr}}$), 1.07 (d, ^3J = 6.4 Hz, 3H, C$H_{3\text{-}i\text{Pr}}$), 1.02 (d, ^3J = 6.5 Hz, 3H, C$H_{3\text{-}i\text{Pr}}$), 0.96 (t, ^3J = 7.7 Hz, 3H, C8-C$H_{3\text{-Et}}$), 0.93 (two overlapping t, ^3J = 7.7 Hz, 6H, C7-C$H_{3\text{-Et}}$) and C10-C$H_{3\text{-Et}}$), 0.62 (d, ^3J = 6.5 Hz, 3H, C$H_{3\text{-}i\text{Pr}}$). **^{11}B NMR** (193 MHz, benzene-d_6): δ (ppm) = 69.3 (br, B2, fwhm ≈ 1550 Hz), 1.5 (B1). **^{13}C{^{1}H,^{11}B} NMR** (151 MHz, benzene-d_6): δ (ppm) = 212.3 (C9), 159.3 (B1C_{carbene}), 152.6 (C1), 150.7 (C10), 149.6 (B2C_{carbene}), 146.8 (C6), 132.2 (CH$_{\text{Bn}}$), 128.1 (CH$_{\text{Bn}}$), 126.9 (CH$_{\text{Bn}}$), 123.3 (CH$_{\text{Bn}}$), 121.1 (NCH), 120.8 (NCH), 119.7 (NCH), 119.3 (NCH), 71.7 (C8), 67.5 (C7), 53.5 (NCH$_{i\text{Pr}}$), 52.8 (NCH$_{i\text{Pr}}$), 51.1 (NCH$_{i\text{Pr}}$), 50.9 (NCH$_{i\text{Pr}}$), 28.0 (C8-CH$_{2\text{-Et}}$), 27.0 (C9-CH$_{2\text{-Et}}$), 24.6 (CH$_{3\text{-}i\text{Pr}}$), 24.5 (CH$_{3\text{-}i\text{Pr}}$), 24.3 (CH$_{3\text{-}i\text{Pr}}$), 24.1 (CH$_{3\text{-}i\text{Pr}}$), 24.0 (CH$_{3\text{-}i\text{Pr}}$), 23.7 (CH$_{3\text{-}i\text{Pr}}$), 23.7 (C7-CH$_{2\text{-Et}}$), 21.9 (C10-CH$_{2\text{-Et}}$), 21.5 (CH$_{3\text{-}i\text{Pr}}$), 15.4 (C10-CH$_{3\text{-Et}}$), 13.0 (C8-CH$_{3\text{-Et}}$), 12.2 (C9-CH$_{3\text{-Et}}$), 9.51 (C7-CH$_{3\text{-Et}}$). **HRMS LIFDI** (*m/z*) for $[C_{36}H_{56}B_2ClN_4]^+ = [M - Cl]^+$: calcd. 601.4374; found 601.4357.

NMR spectra of isolated compounds

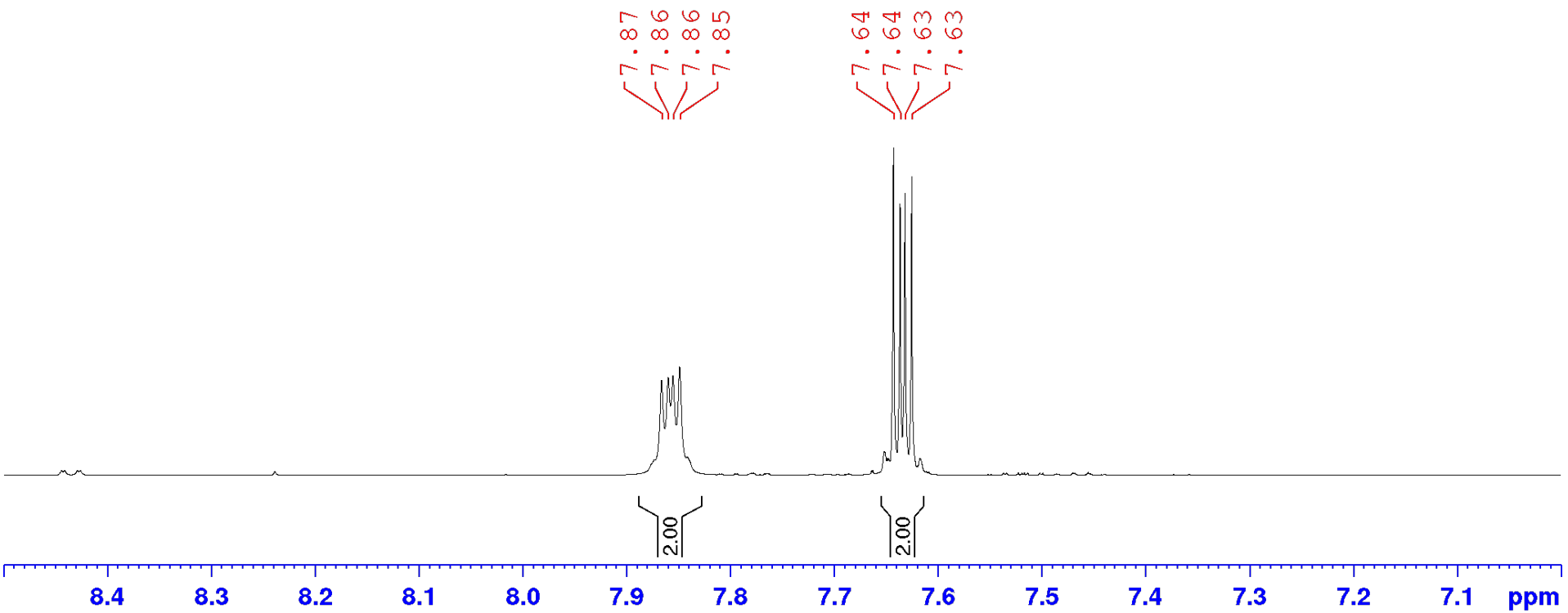

Figure S1. ^{1}H NMR spectrum of $\mathbf{1}^{\mathbf{Bz}}$ in CD_2Cl_2.

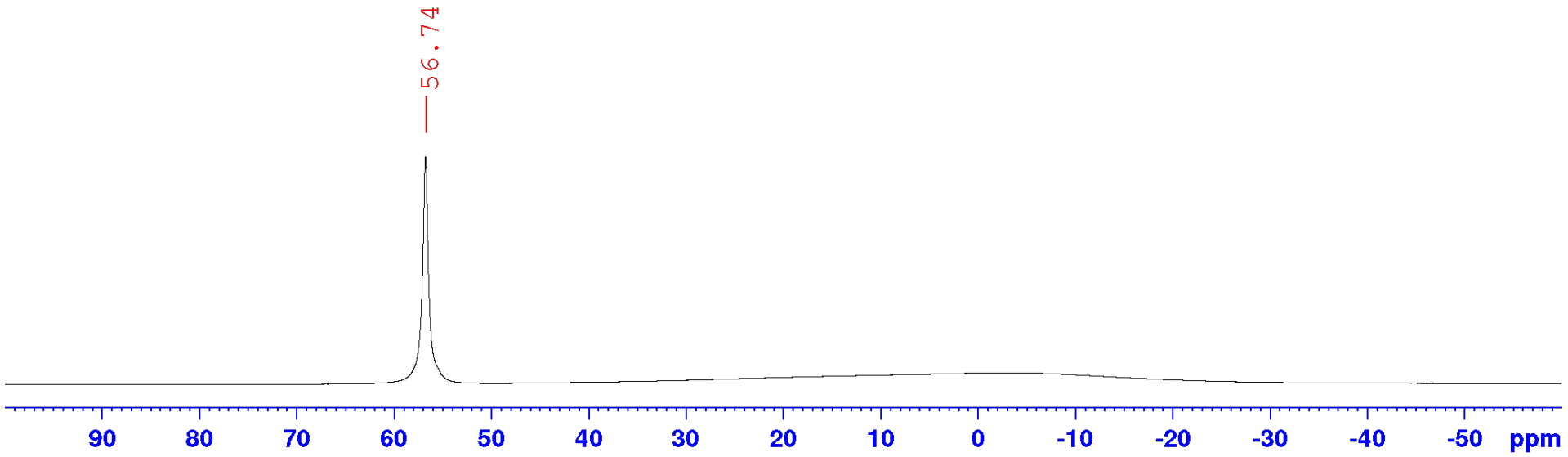

Figure S2. ^{11}B NMR spectrum of $\mathbf{1}^{Bz}$ in CD_2Cl_2.

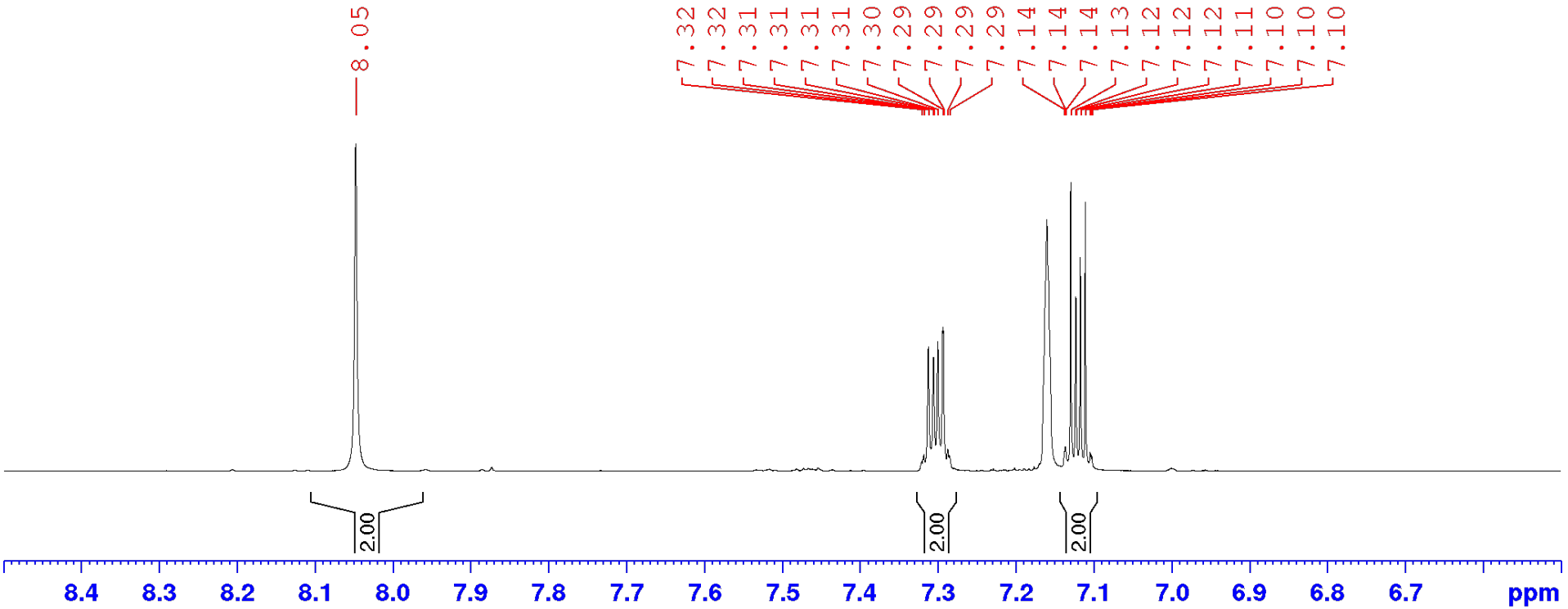

Figure S3. ^{1}H NMR spectrum of **1**$^{\mathbf{Naph}}$ in C_6D_6.

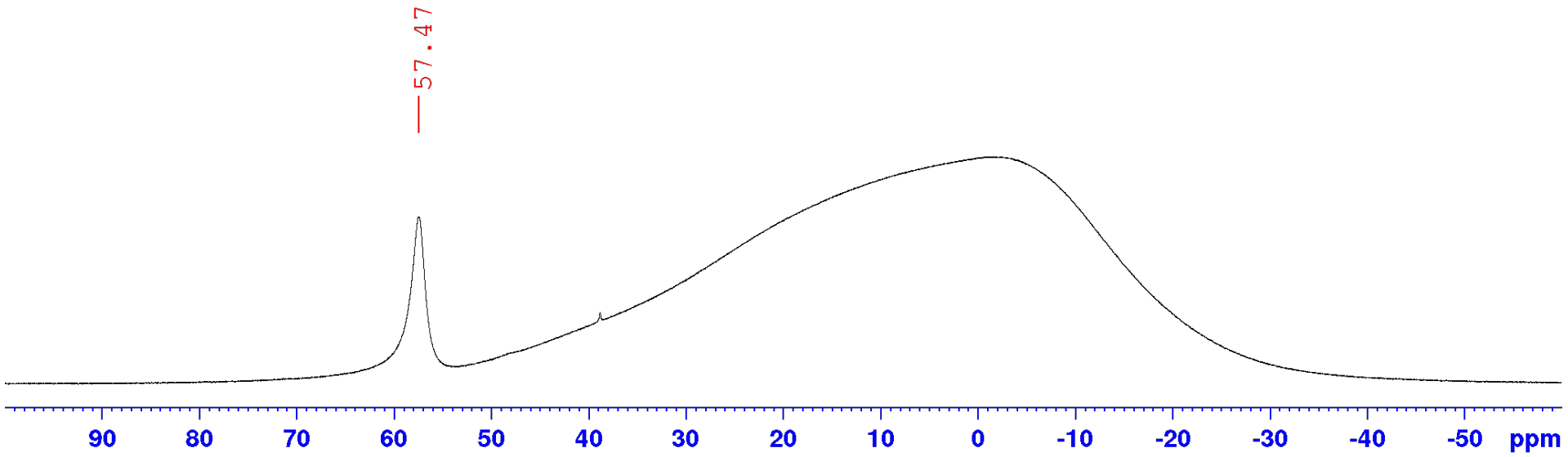

Figure S4. ^{11}B NMR spectrum of $\mathbf{1}^{\mathbf{Naph}}$ in C_6D_6.

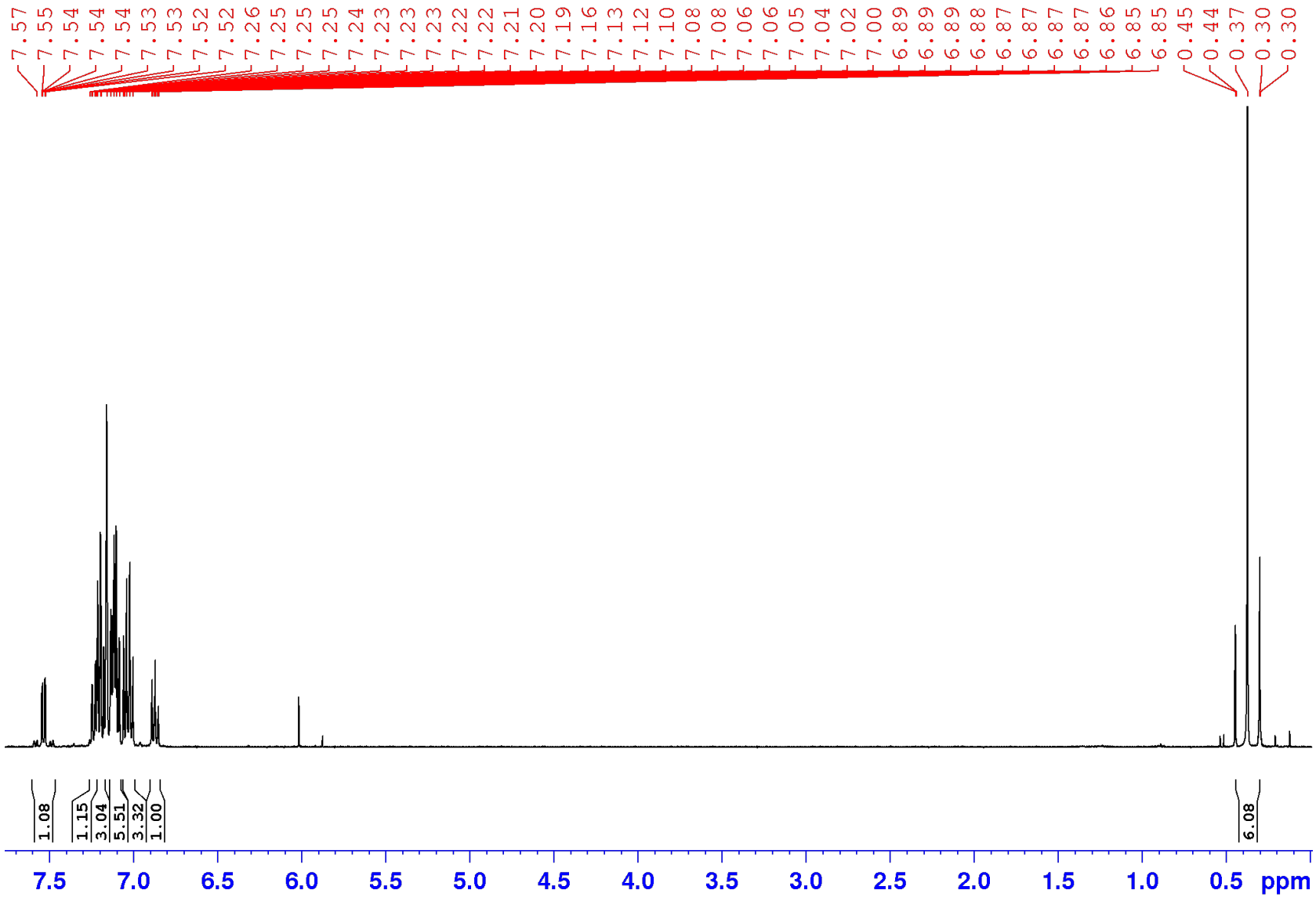

Figure S5. ^{1}H NMR spectrum of **2-BzPh** in C_6D_6.

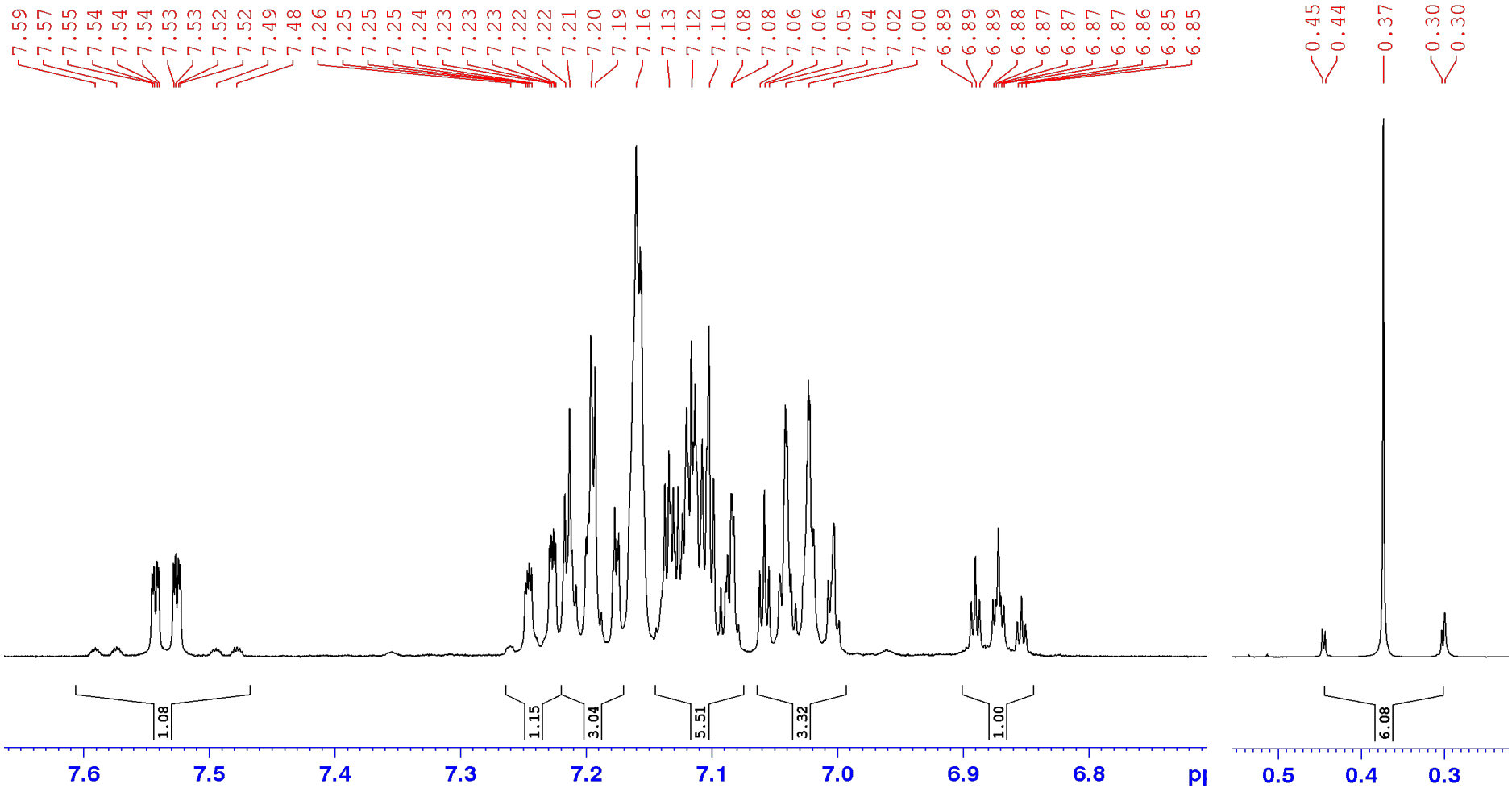

Figure S6. Expansion of the aromatic (left) and aliphatic (right) regions of the ^{1}H NMR spectrum of **2-BzPh** in C_6D_6.

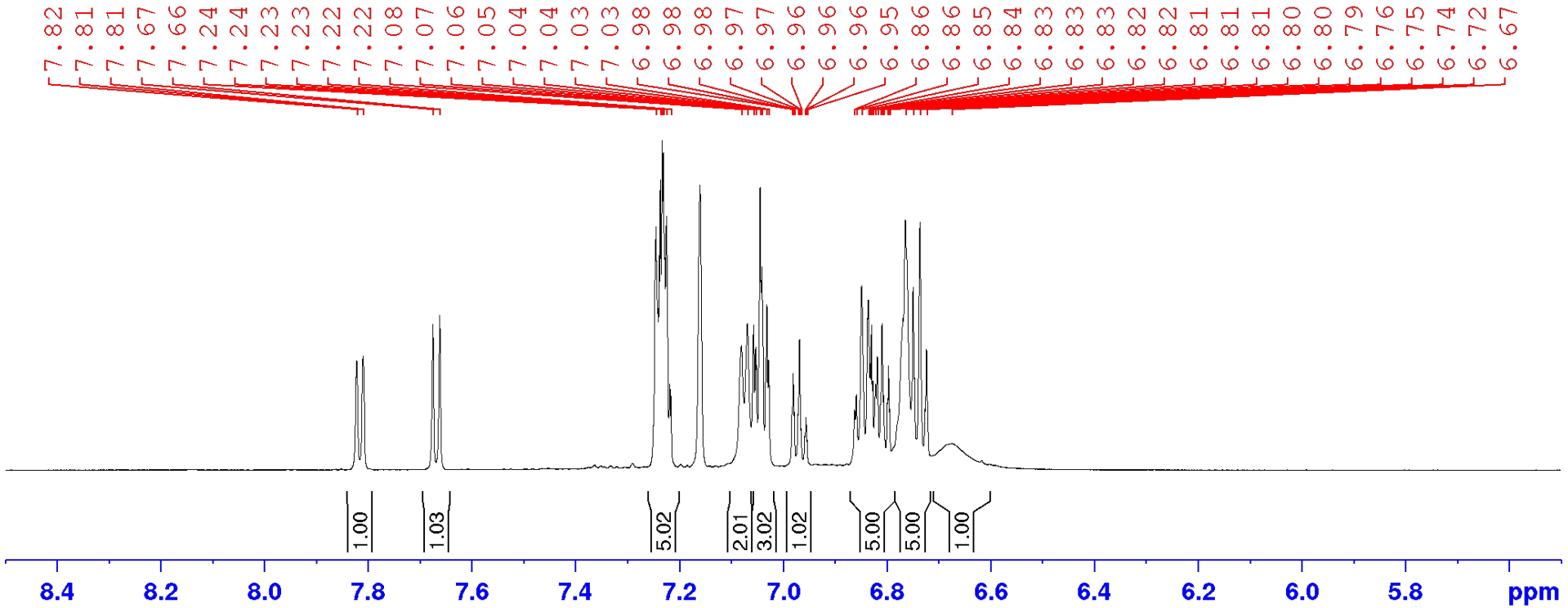

Figure S7. ^{1}H NMR spectrum of **3^{Bz}-Ph** in C_6D_6.

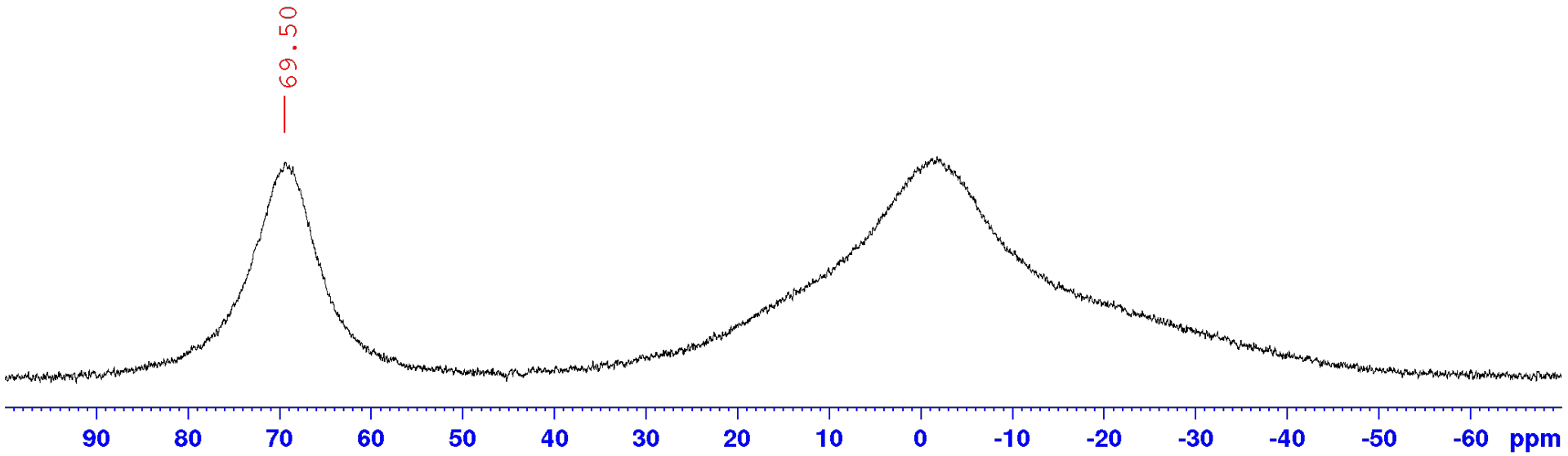

Figure S8. ^{11}B NMR spectrum of **3^{Bz}-Ph** in C_6D_6 (acquired with reduced background, SFO1 = 192.6 MHz).

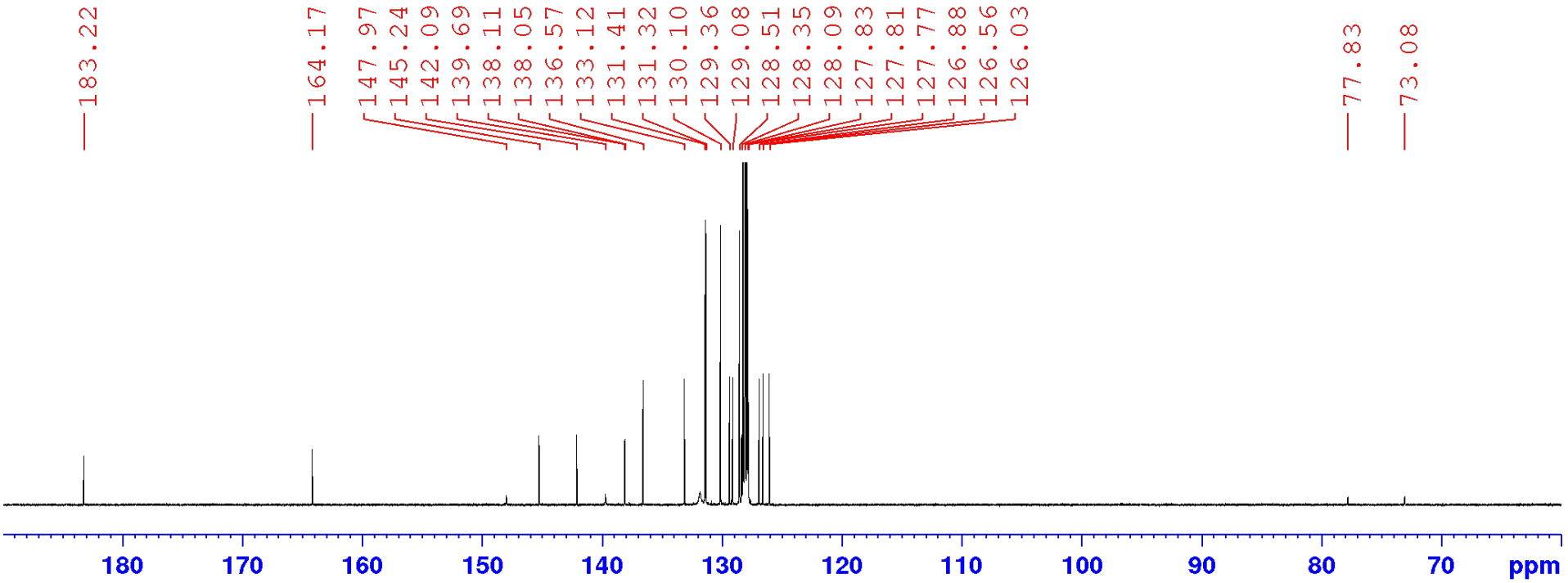

Figure S9. $^{13}C\{^{1}H,^{11}B\}$ NMR spectrum of **3^{Bz}-Ph** in C_6D_6.

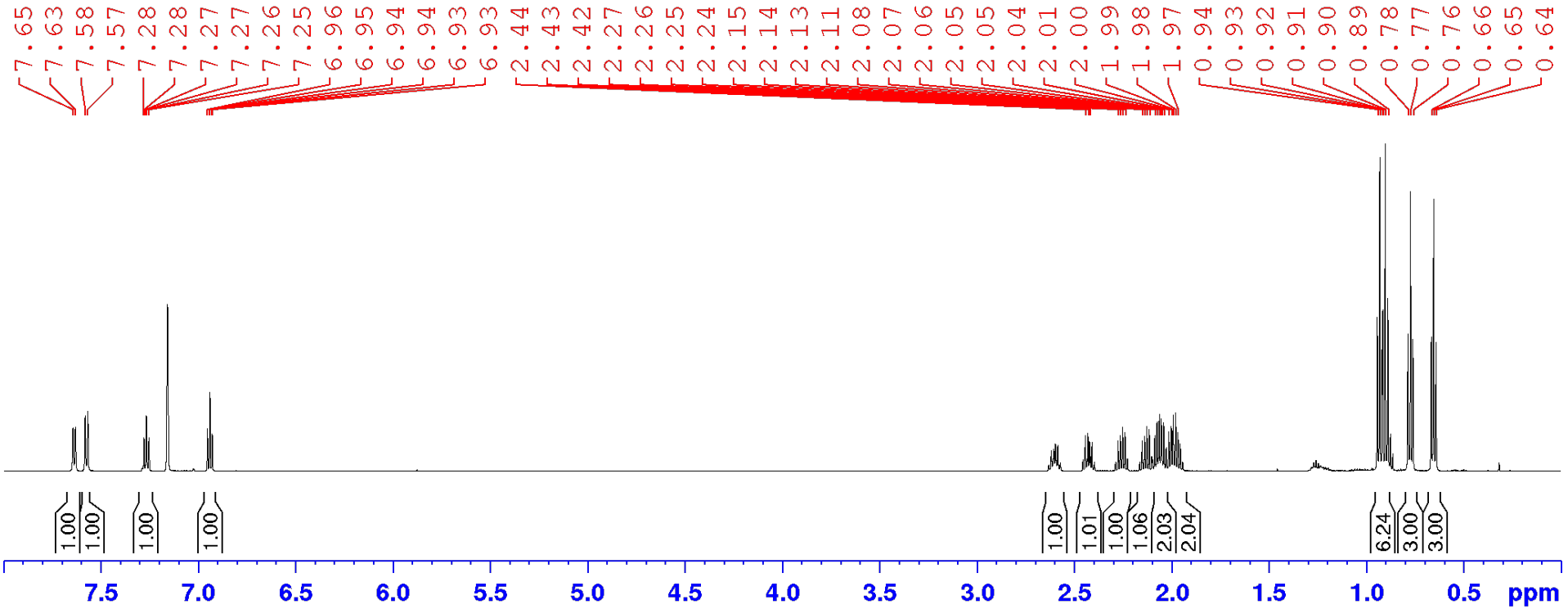

Figure S10. ^{1}H NMR spectrum of **3^{Bz}-Et** in C_6D_6. The additional resonances around 0.8 (t) and 1.3 (m) ppm result from residual pentane used for washing.

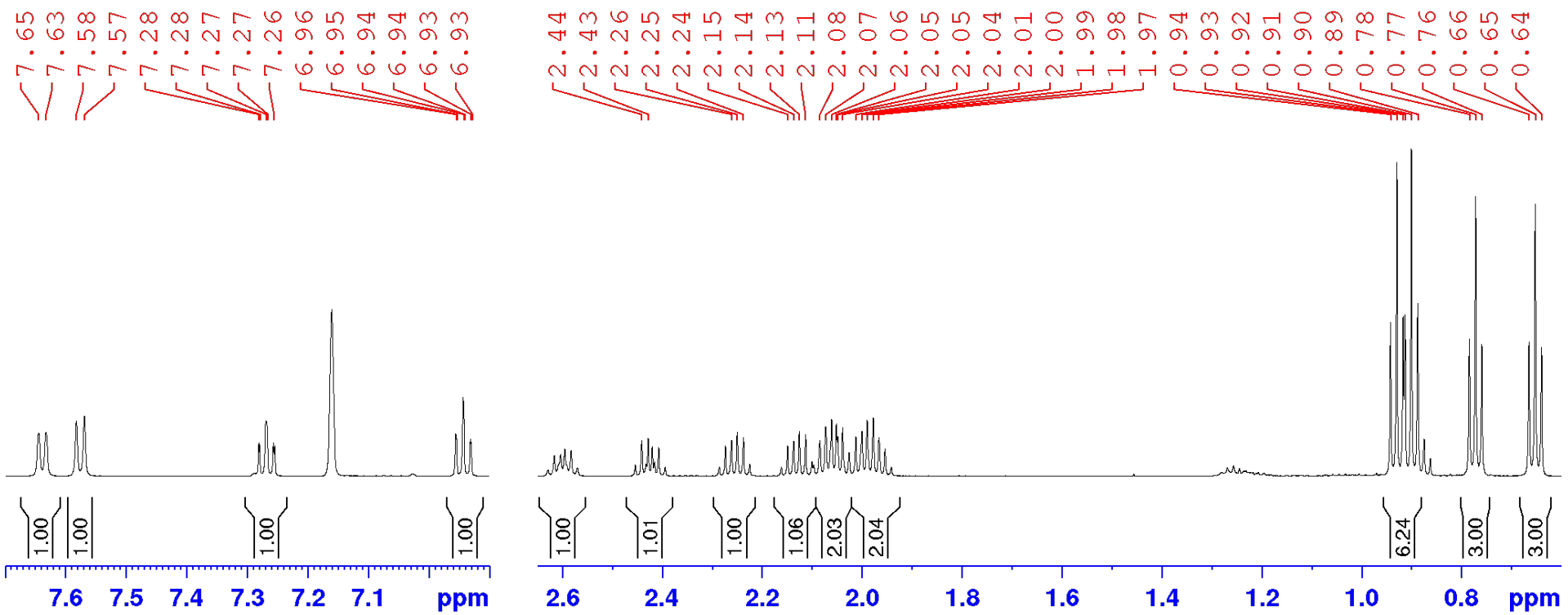

Figure S11. Expansion of the aromatic (left) and aliphatic (right) regions of the ^{1}H NMR spectrum of **3Bz-Et** in C_6D_6.

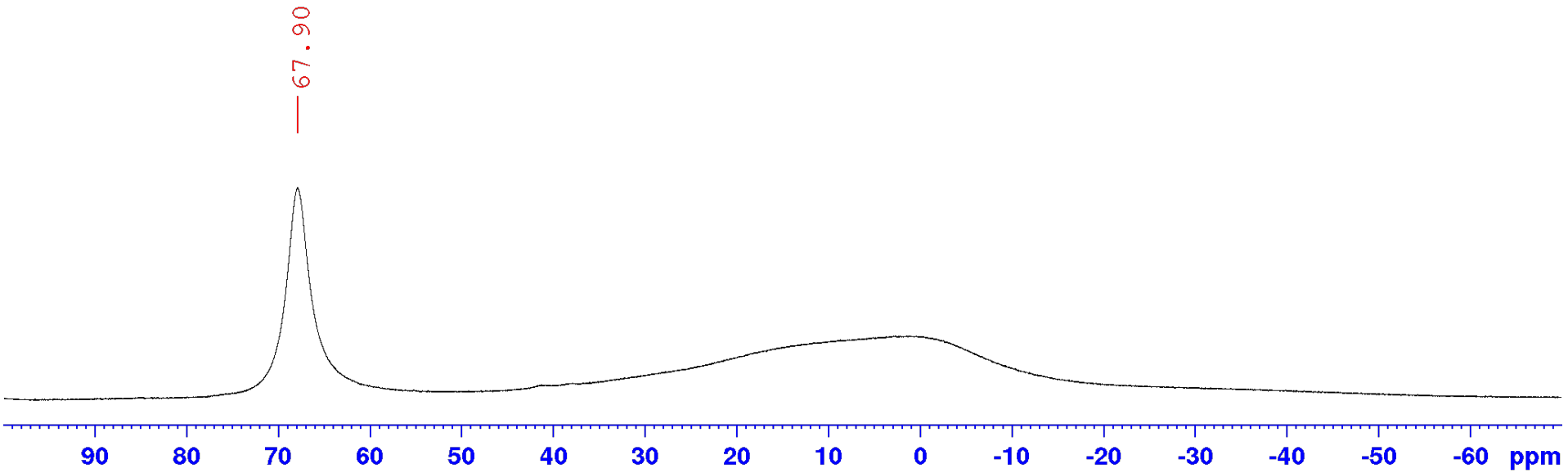

Figure S12. ^{11}B NMR spectrum of **3^{Bz}-Et** in C_6D_6.

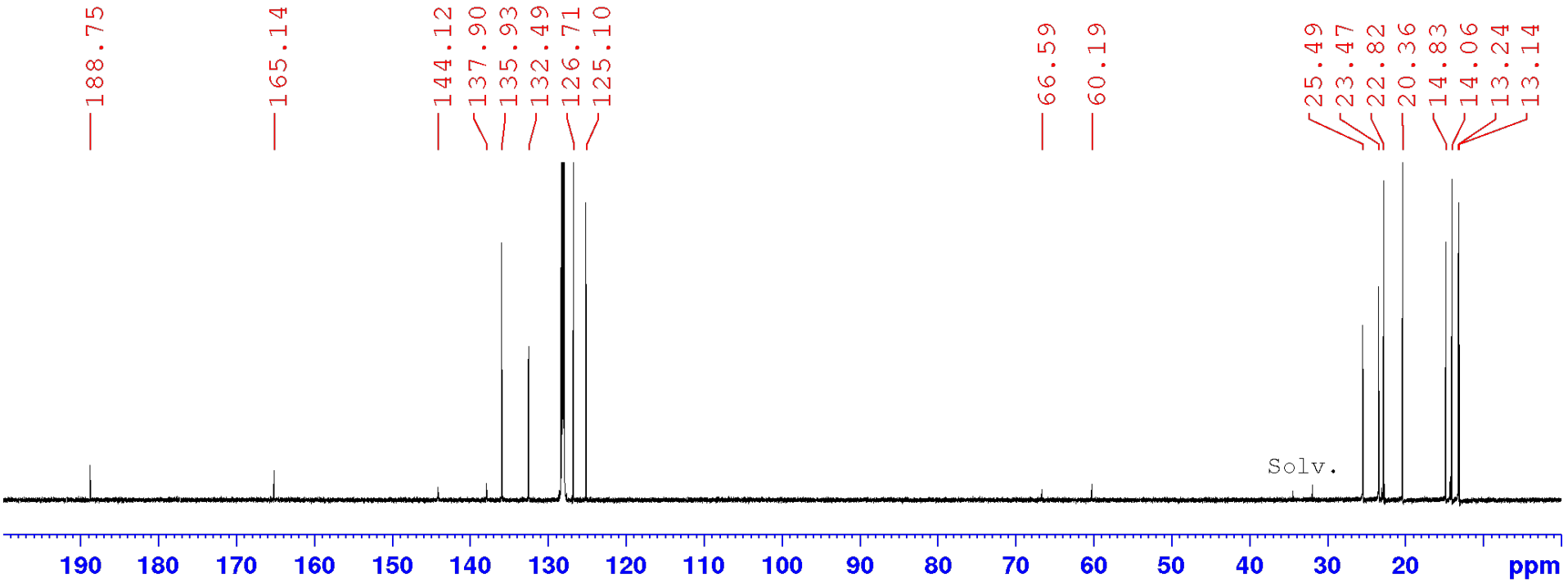

Figure S13. $^{13}C\{^{1}H,^{11}B\}$ NMR spectrum of **3^{Bz}-Et** in C_6D_6.

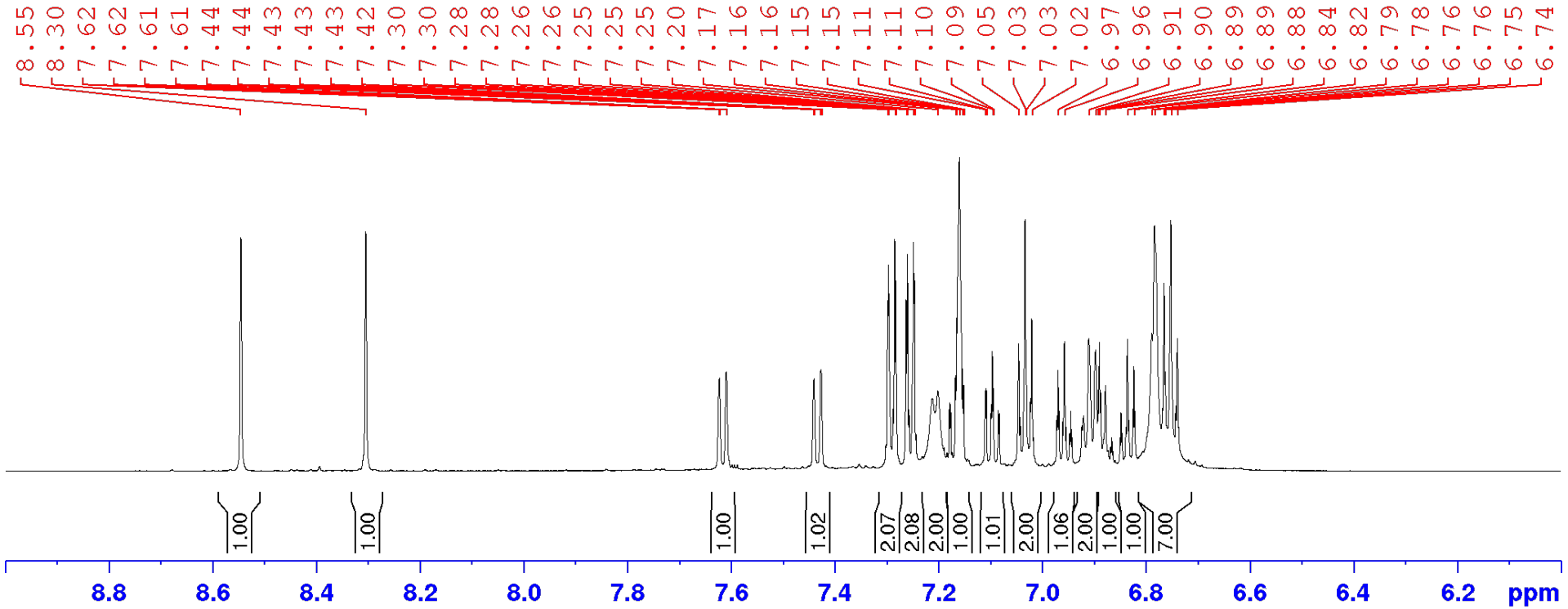

Figure S14. ^{1}H NMR spectrum of **3^{Naph}-Ph** in C_6D_6.

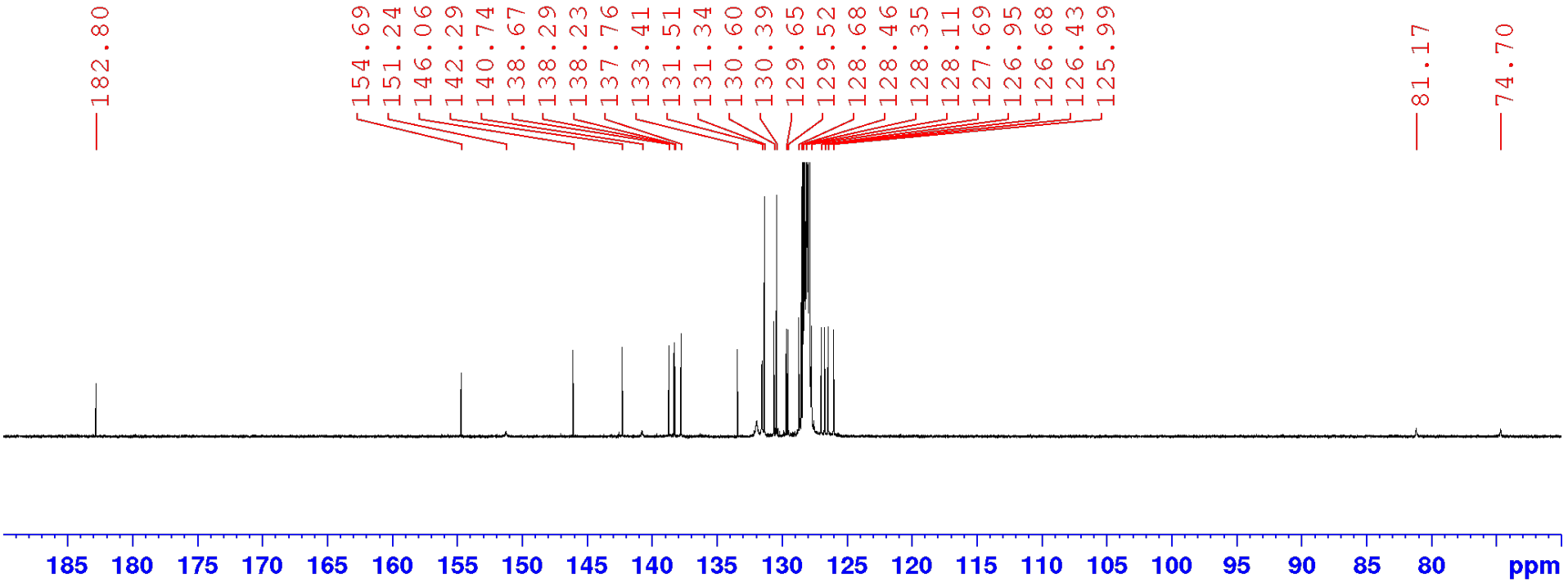

Figure S15. $^{13}C\{^{1}H\}$ NMR spectrum of **3^{Naph}-Ph** in C_6D_6.

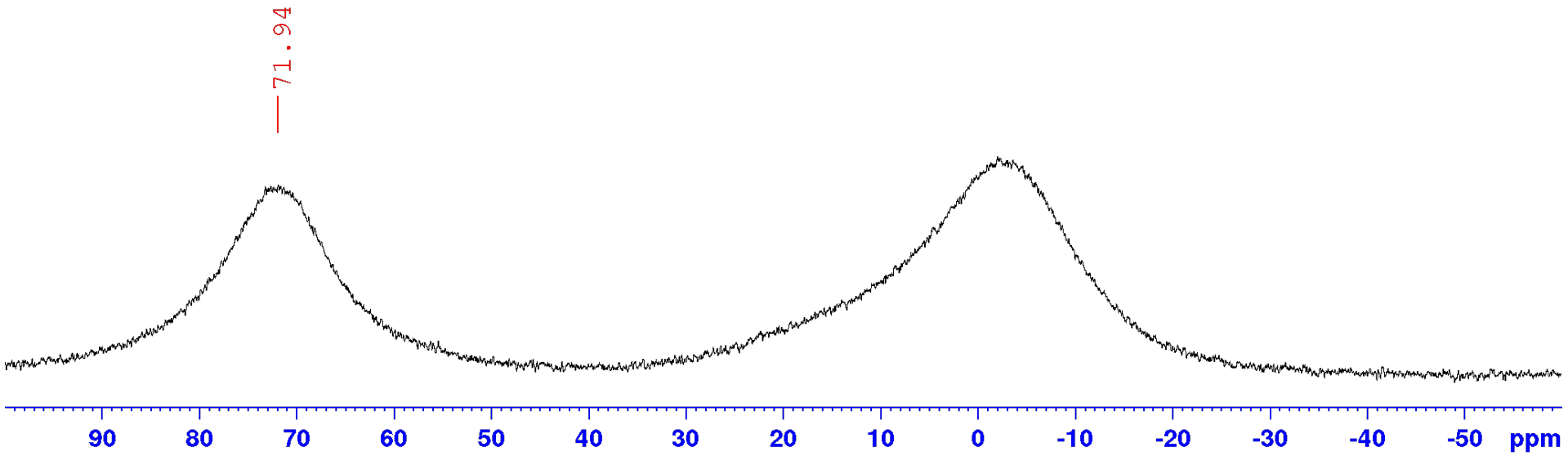

Figure S16. ^{11}B NMR spectrum of **3^{Naph}-Ph** in C_6D_6 (including background reduction, signal at ca. 0 ppm arises from the spectrometer probehead).

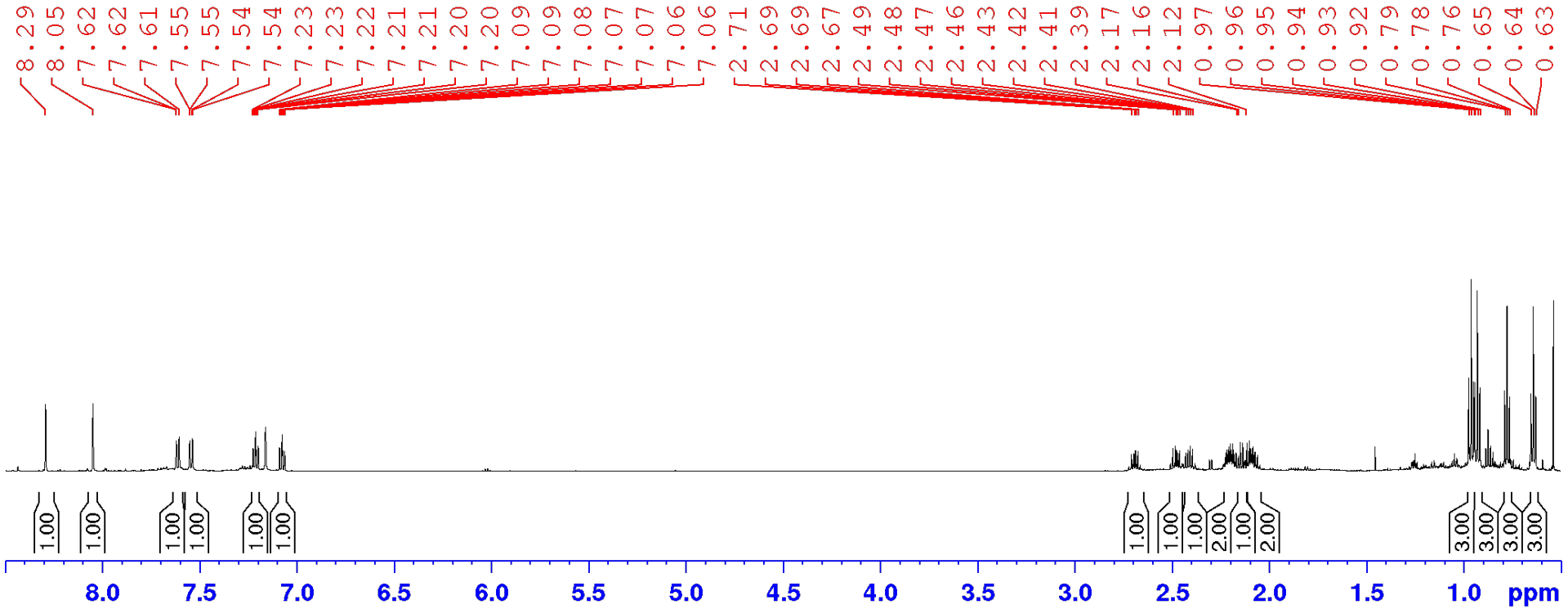

Figure S17. ^{1}H NMR spectrum of **3^{Naph}-Et** in C_6D_6.

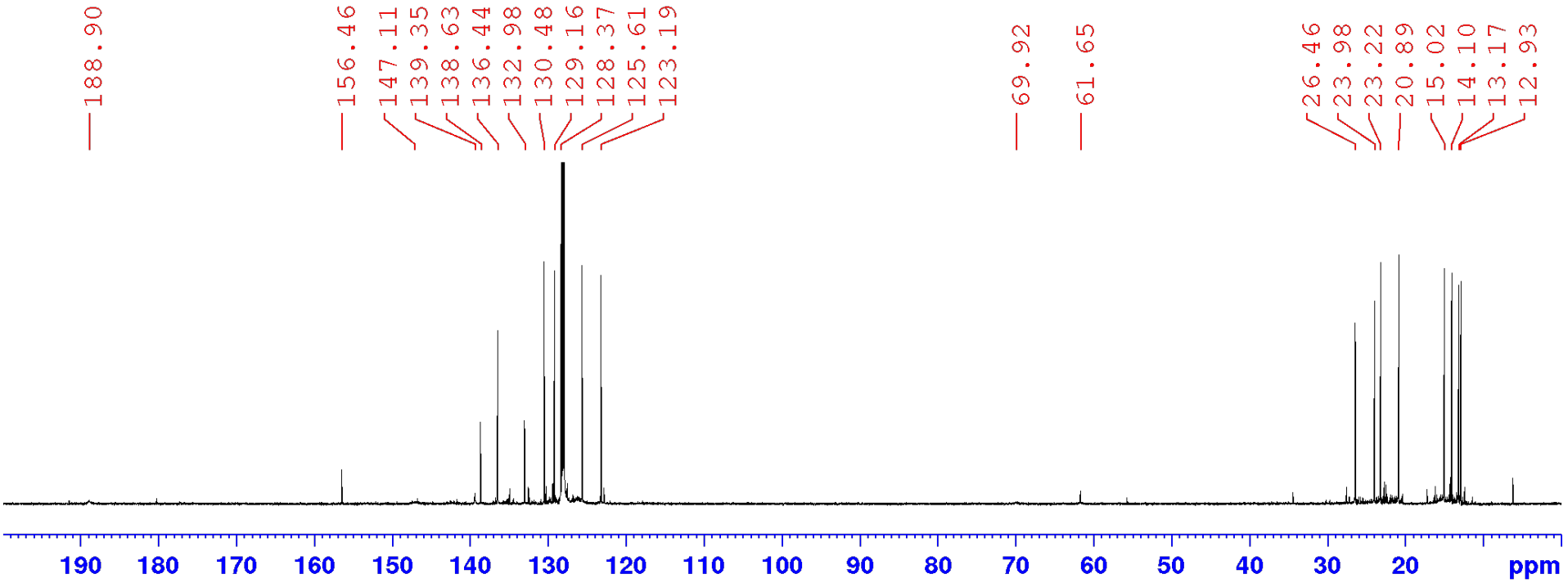

Figure S18. $^{13}C\{^{1}H,^{11}B\}$ NMR spectrum of **3^{Naph}-Et** in C_6D_6.

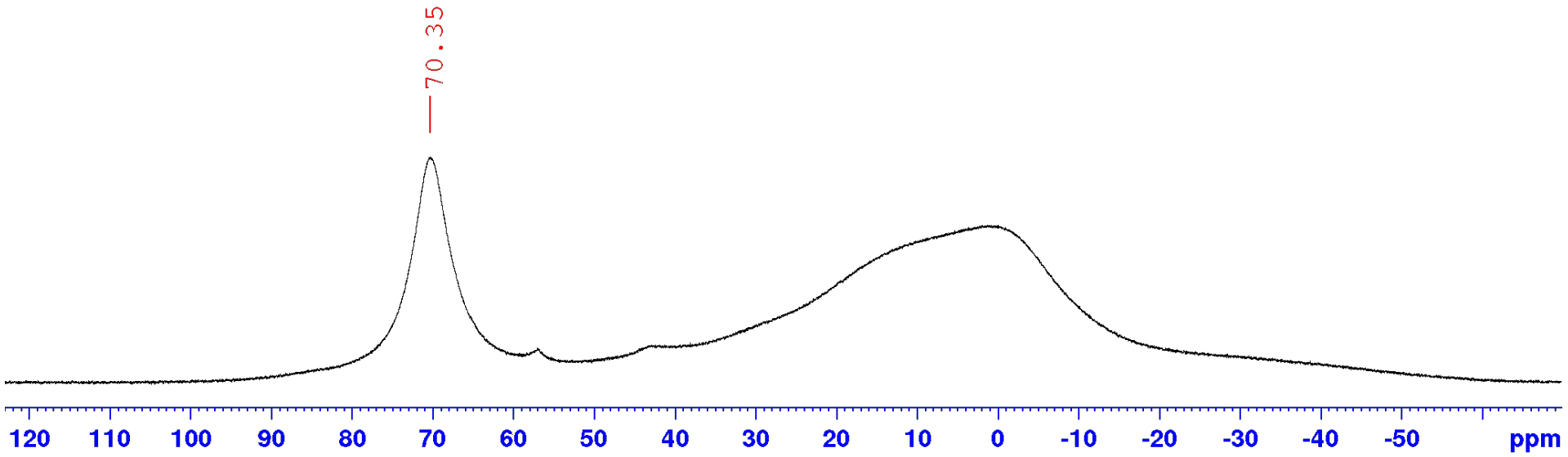

Figure S19. ^{11}B NMR spectrum of **3^{Naph}-Et** in C_6D_6.

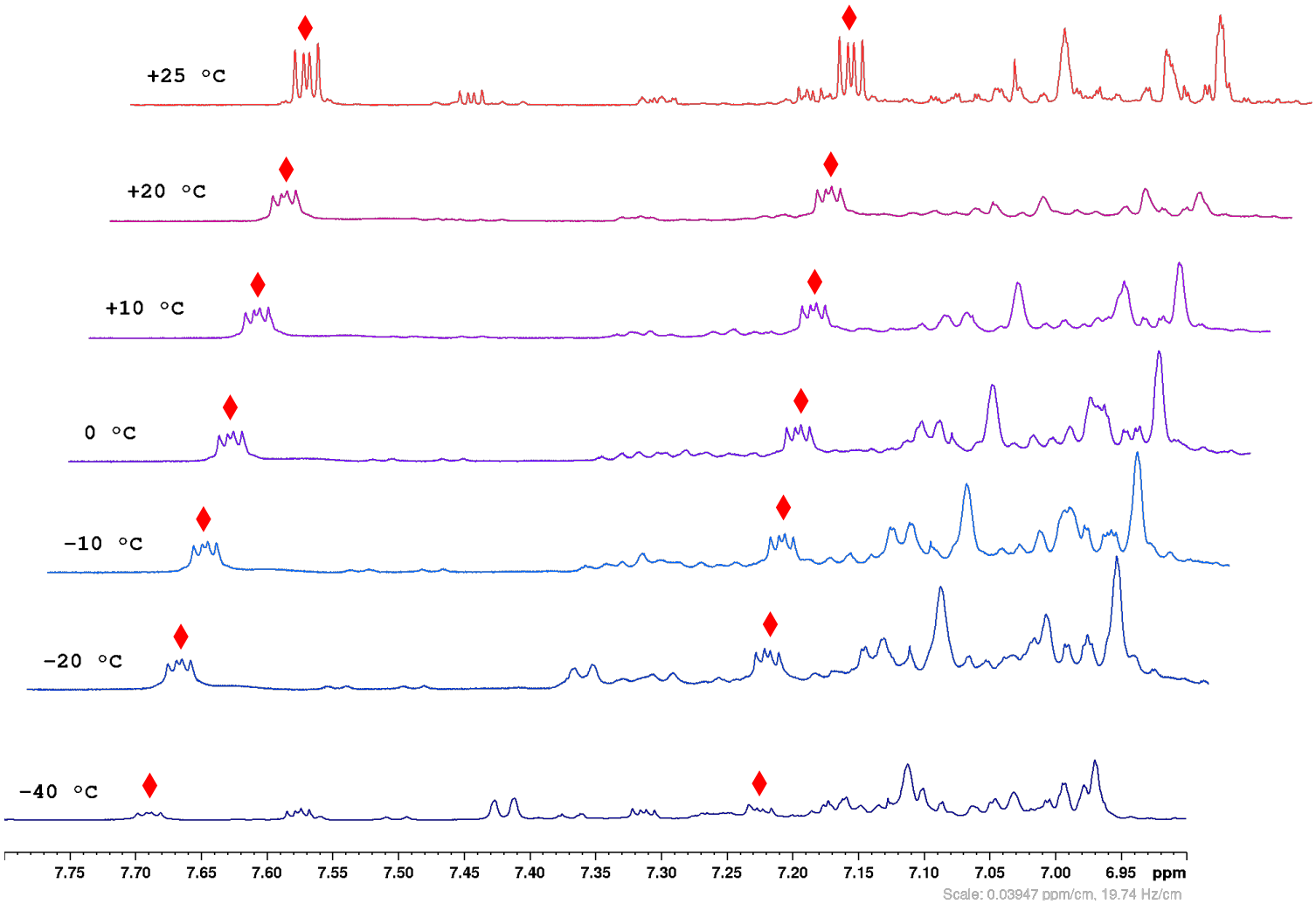

Figure S20. Stack-plot of the aryl region of the ^{1}H NMR spectra of 2:1 reaction mixture of **2-Et** and $\mathbf{1}^{\mathbf{Bz}}$ in toluene-d_8 monitored between −40 °C and 25 °C: ♦ = $\mathbf{4}^{\mathbf{Bz}}$**-Et**. The remaining resonances are attributed to unidentified decomposition products.

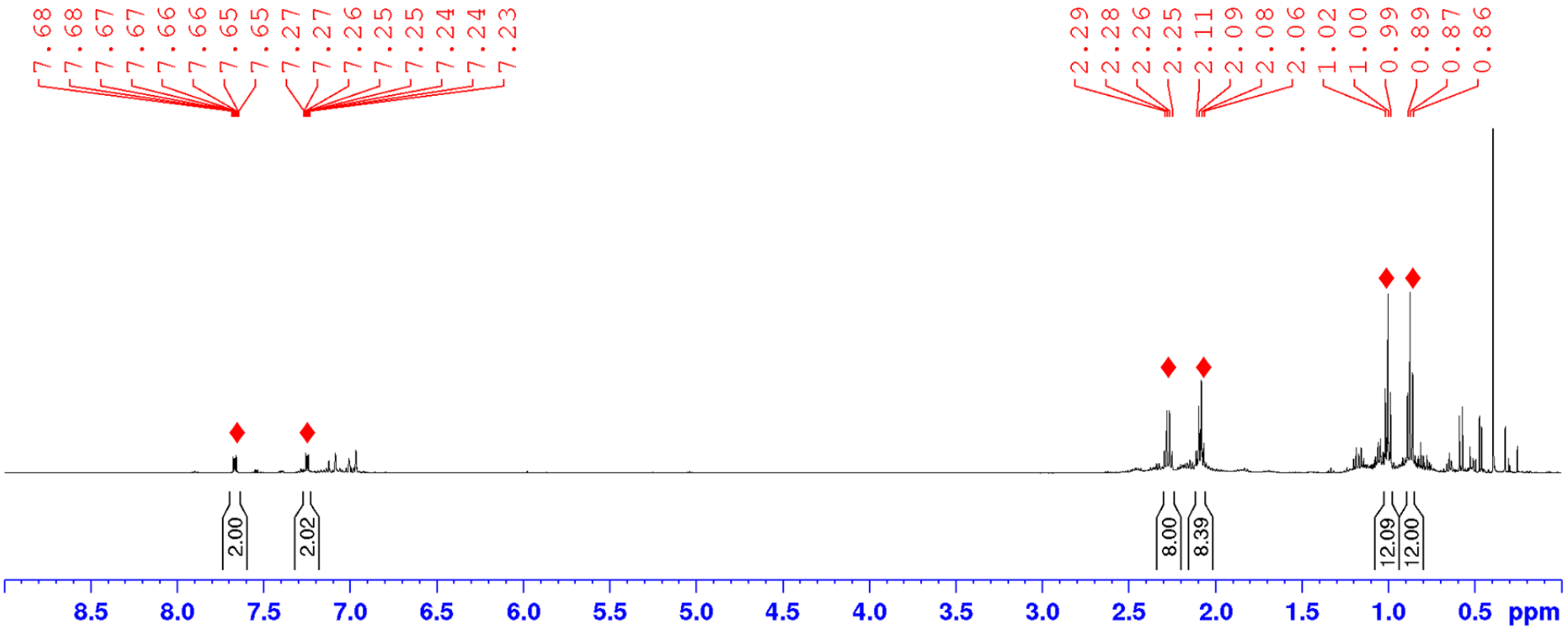

Figure S21. ^{1}H NMR spectrum of the 2:1 reaction mixture of **2-Et** and **1^{Bz}** in toluene-d_8 after slow warming from −40 °C to 25 °C: ♦ = **4^{Bz}-Et**. The remaining resonances are attributed to unidentified decomposition products.

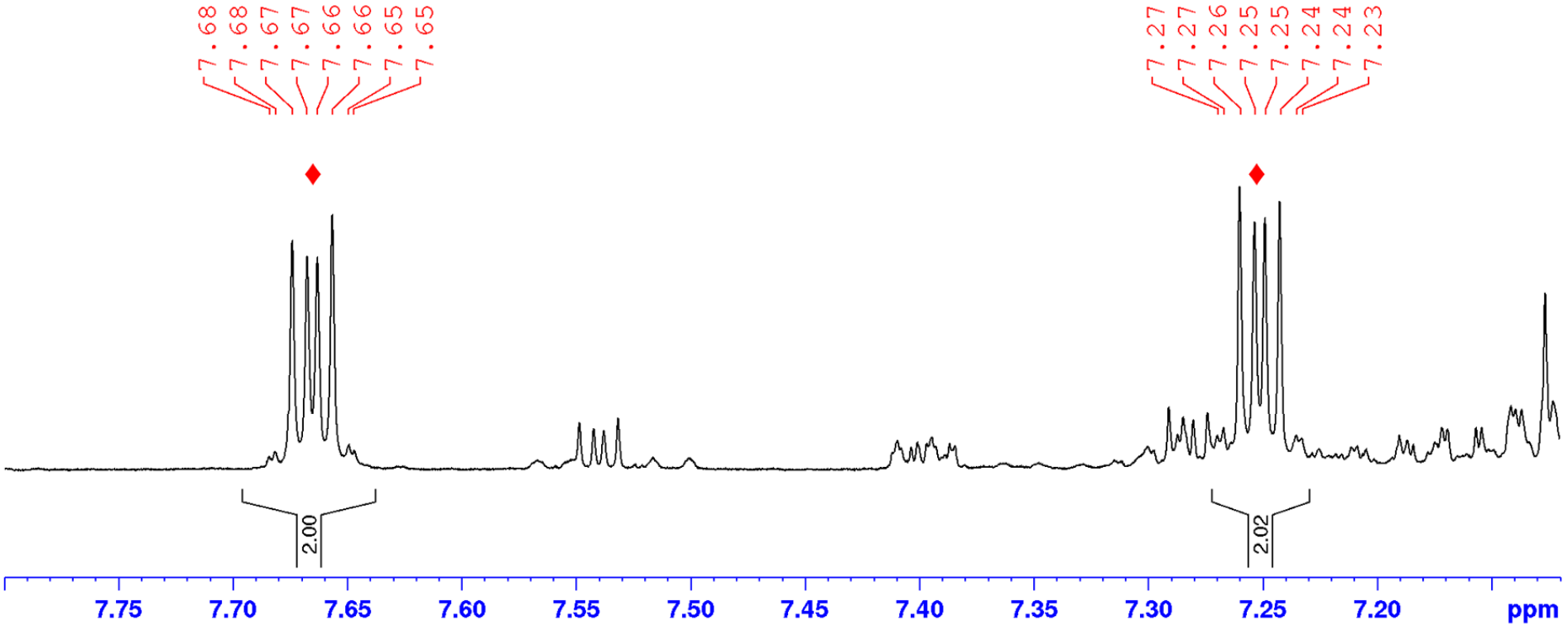

Figure S22. Expansion of the aromatic region of the ^{1}H NMR spectrum of the 2:1 reaction mixture of **2-Et** and **1**$^{\mathbf{Bz}}$ in toluene-d_8 after slow warming from −40 °C to 25 °C: ♦ = **4**$^{\mathbf{Bz}}$**-Et**. The remaining resonances are attributed to unidentified decomposition products.

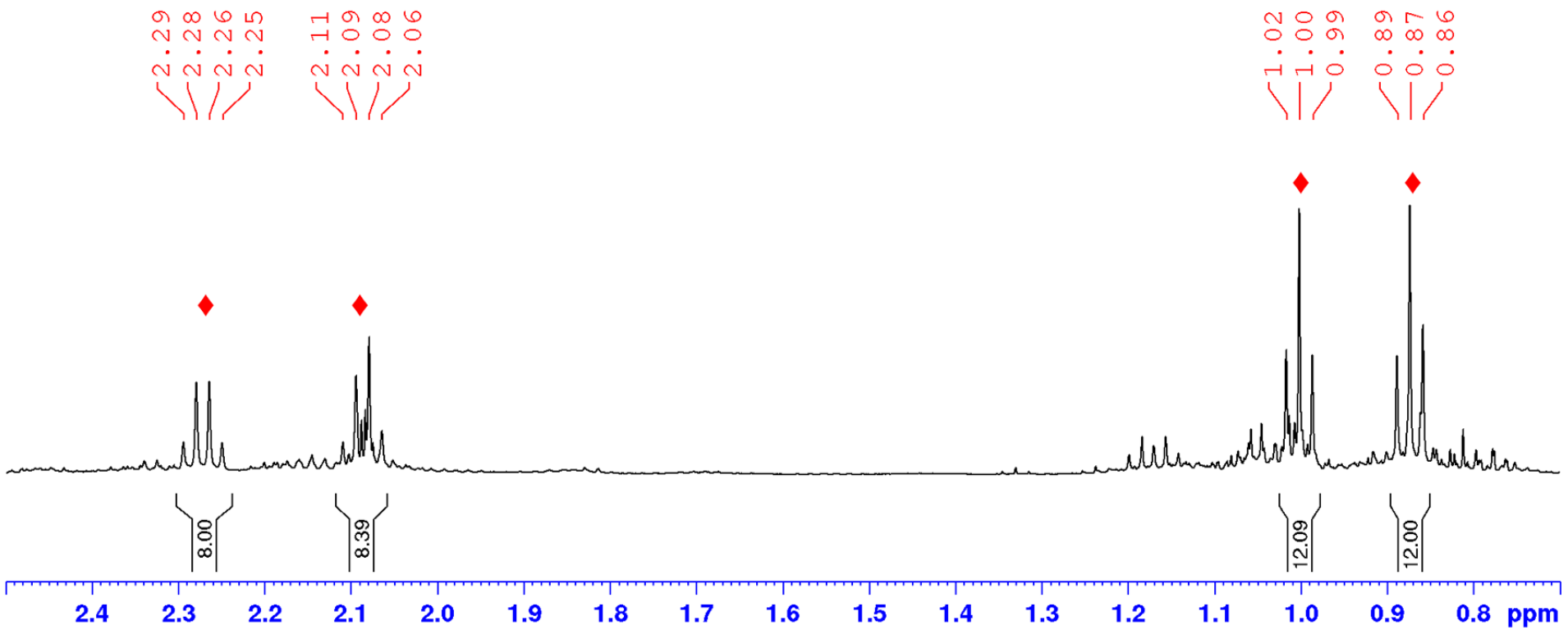

Figure S23. Expansion of the aliphatic region of the ^{1}H NMR spectrum of the 2:1 reaction mixture of **2-Et** and $\mathbf{1^{Bz}}$ in toluene-d_8 after slow warming from −40 °C to 25 °C: ♦ = $\mathbf{4^{Bz}}$**-Et**. The remaining resonances are attributed to unidentified decomposition products.

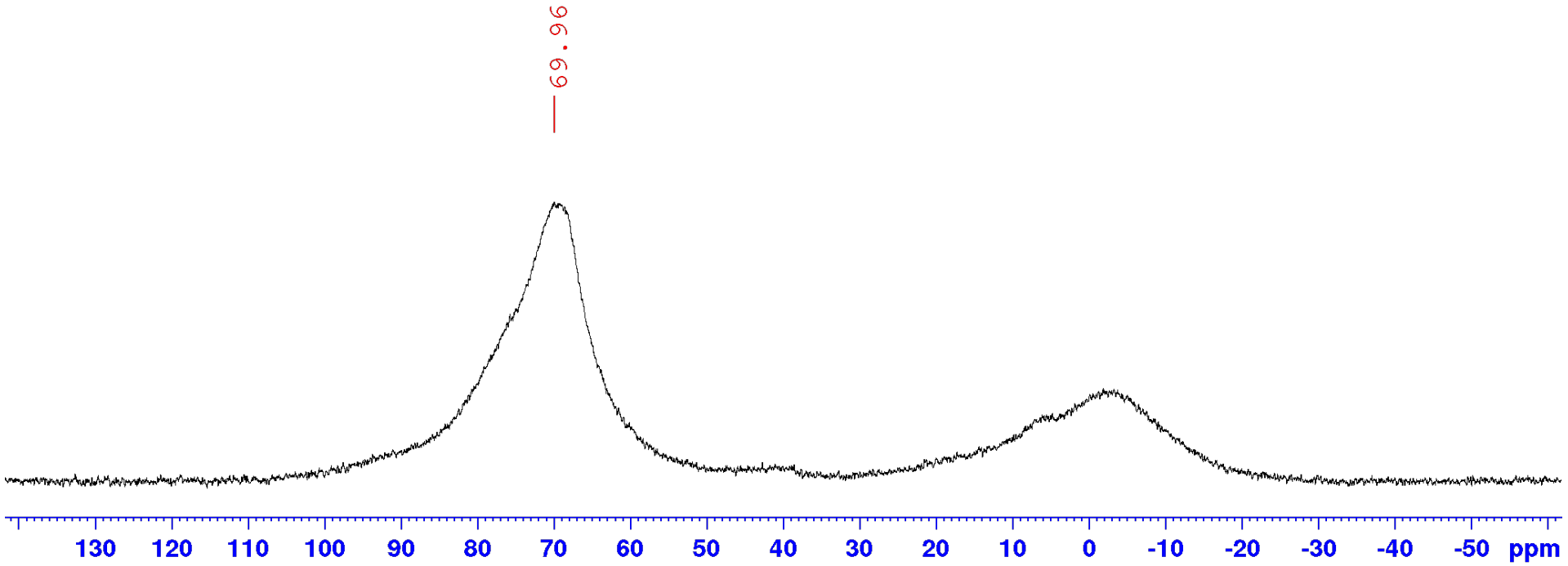

Figure S24. ^{11}B NMR spectrum of the 2:1 reaction mixture of **2-Et** and **1^{Bz}** in toluene-d_8 after slow warming from −40 °C to 25 °C, showing the formation of **4^{Bz}-Et** as the main product (including background reduction, signal at ca. 0 ppm arises from the spectrometer probehead).

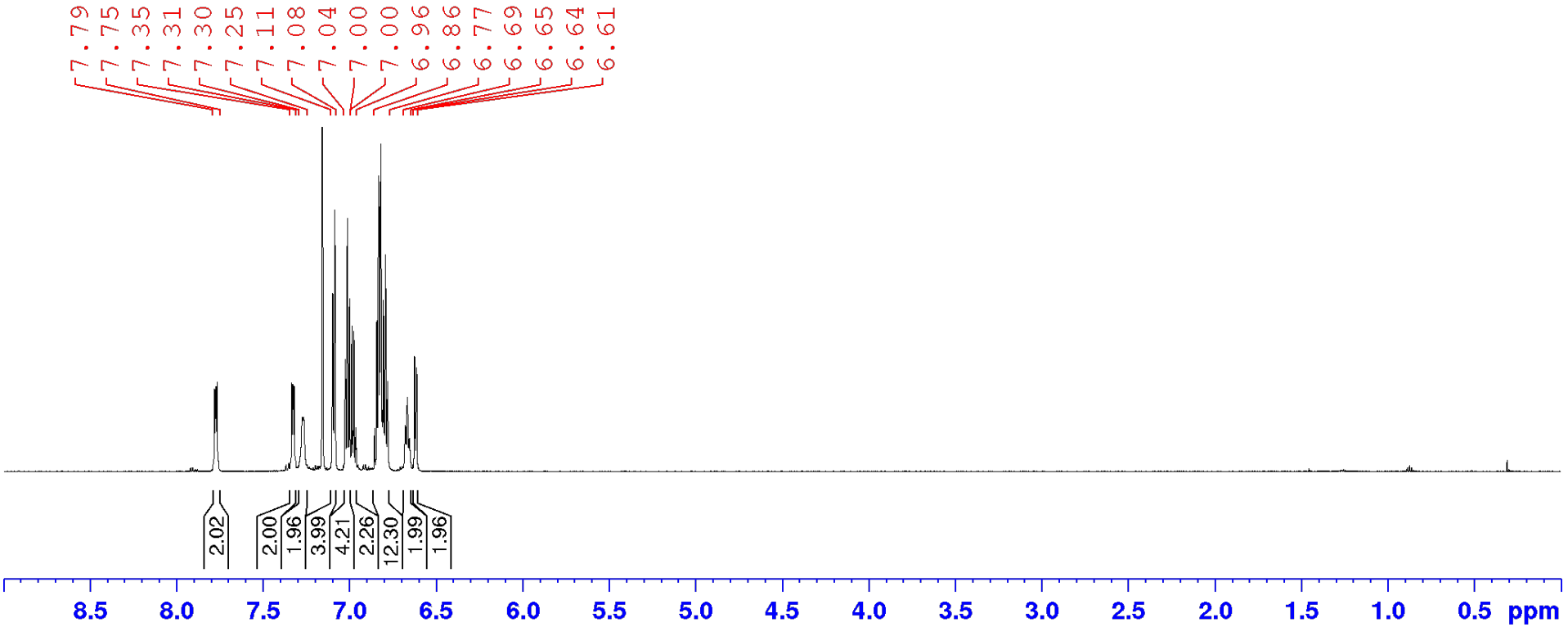

Figure S25. ^{1}H NMR spectrum of **4^{Bz}-BzPh** in C_6D_6.

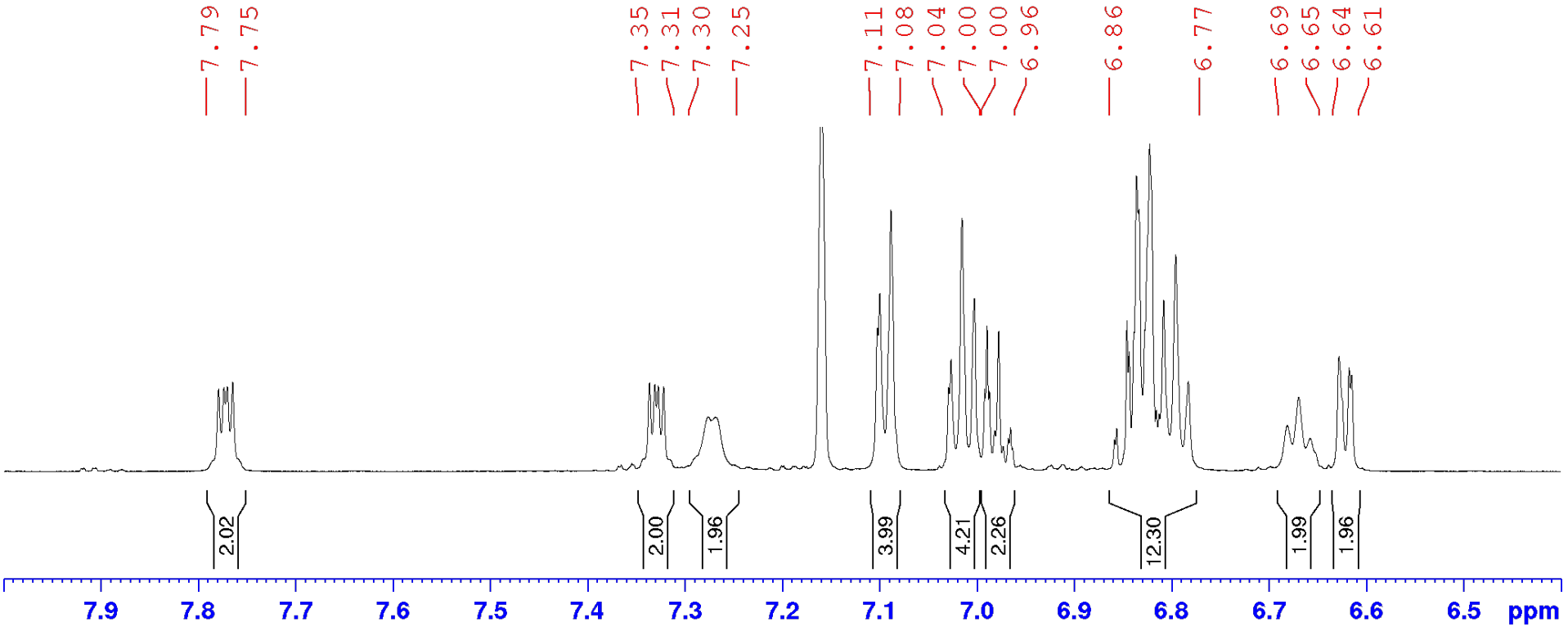

Figure S26. Expansion of the aromatic region of the ^{1}H NMR spectrum of **4^{Bz}-BzPh** in C_6D_6.

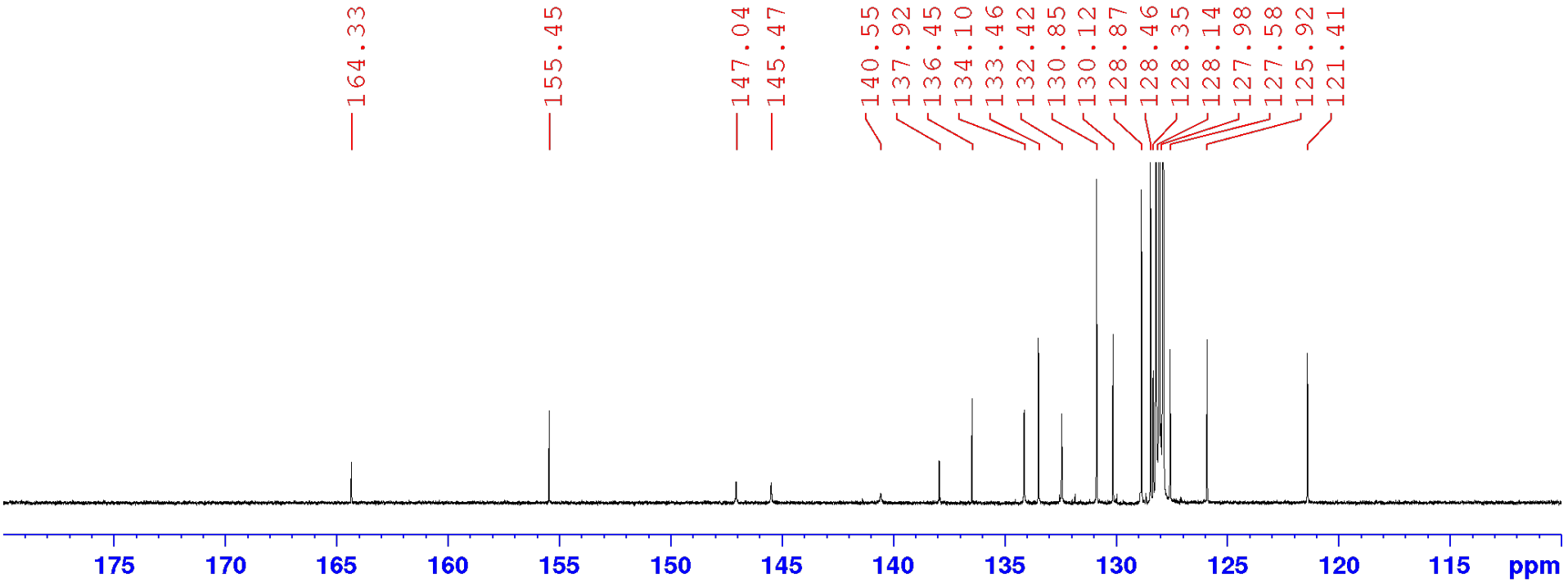

Figure S27. $^{13}C\{^{1}H\}$ NMR spectrum of **4^{Bz}-BzPh** in C_6D_6.

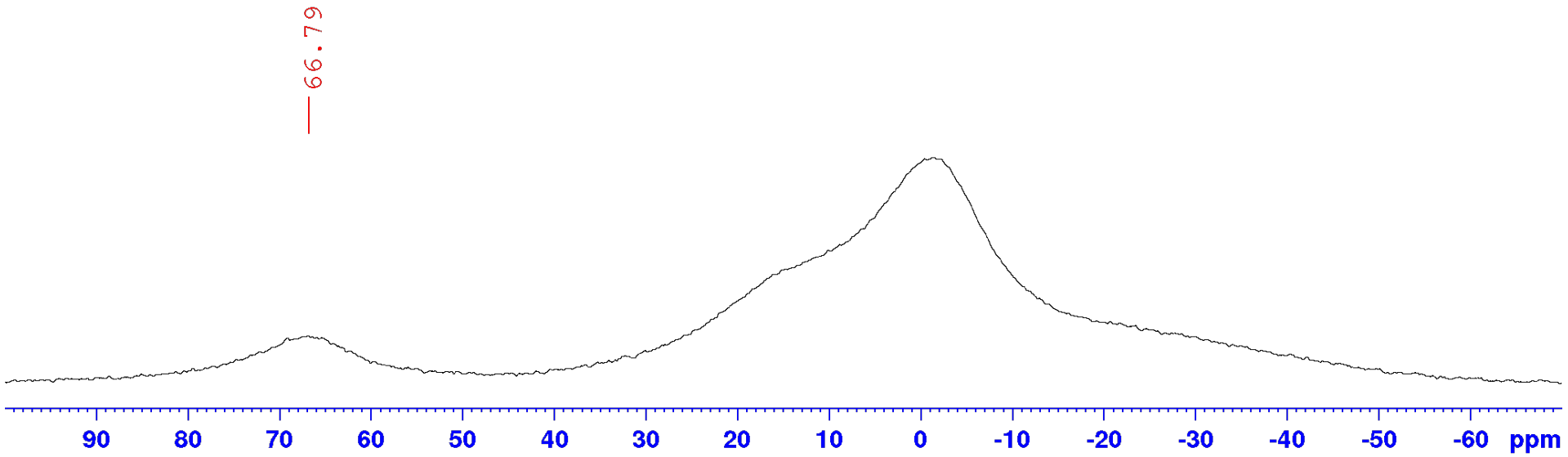

Figure S28. ^{11}B NMR spectrum of **4^{Bz}-BzPh** in C_6D_6 (including background reduction, signal at ca. 0 ppm arises from the spectrometer probehead).

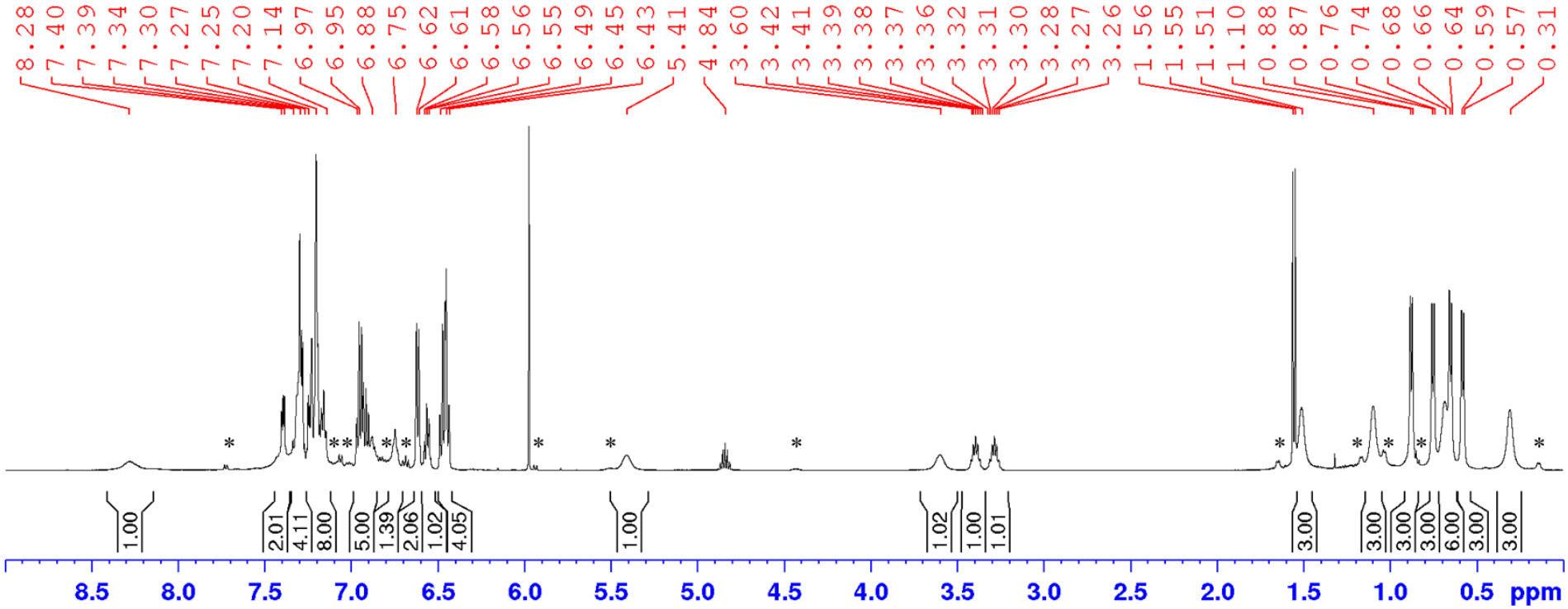

Figure S29. ^{1}H NMR spectrum of **5^{Bz}-Ph** in $C_2D_2Cl_4$. The smaller resonances marked with * are assigned to the rearrangement product **6^{Bz}-Ph**.

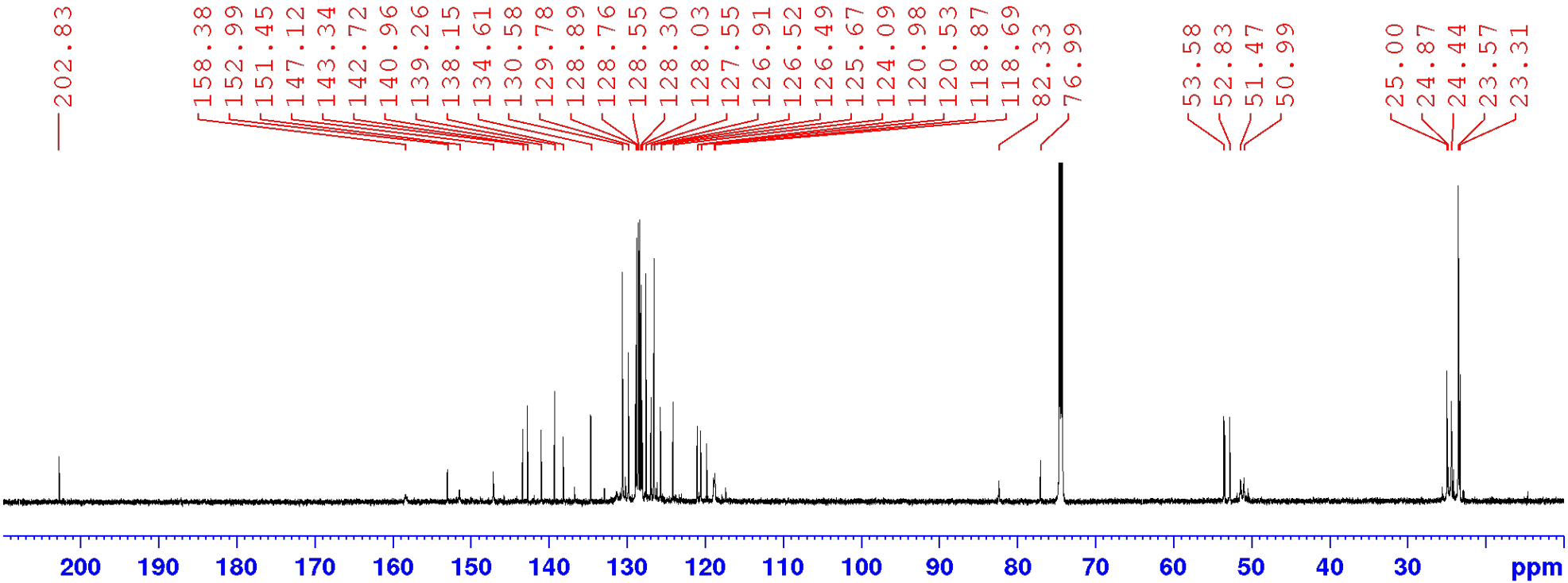

Figure S30. $^{13}C\{^{1}H\}$ NMR spectrum of **5^{Bz}-Ph** in $C_2D_2Cl_4$.

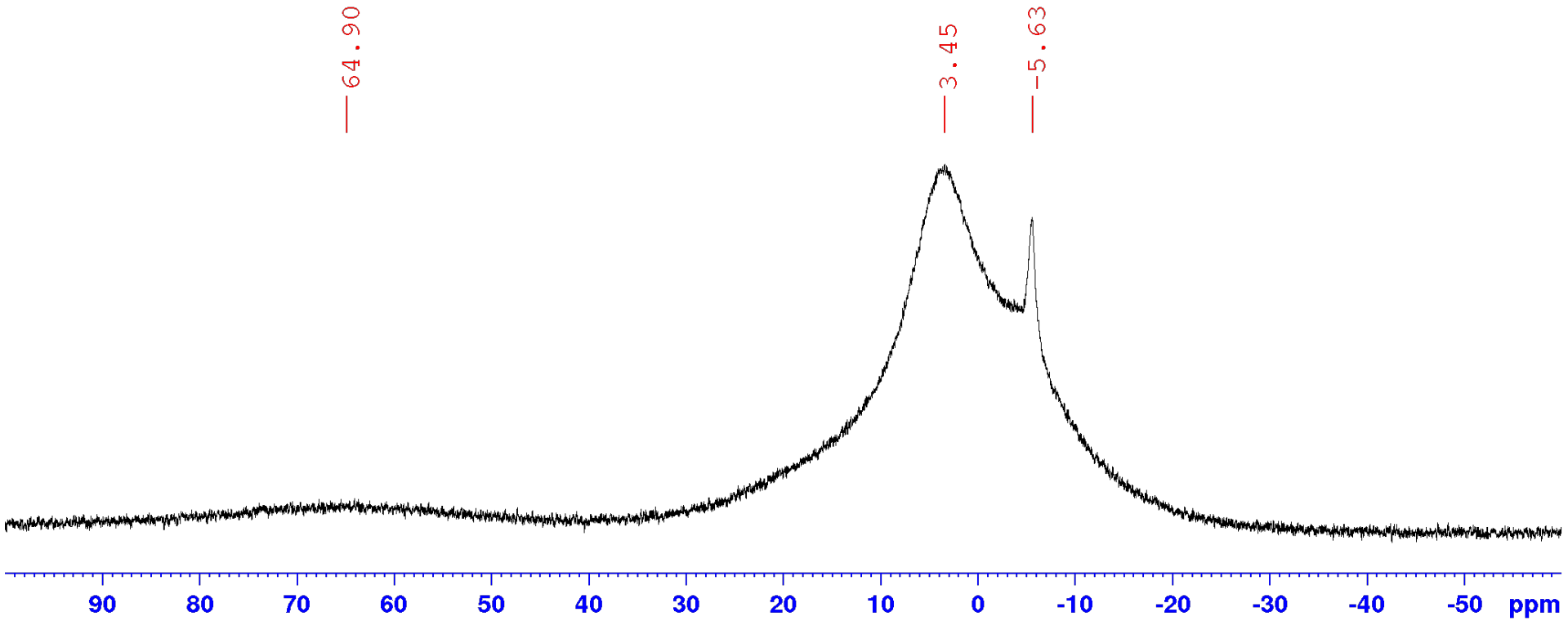

Figure S31. ^{11}B NMR spectrum of **5^{Bz}-Ph** in $C_2D_2Cl_4$. The resonance at –5.6 ppm is assigned to the rearrangement product **6^{Bz}-Ph**.

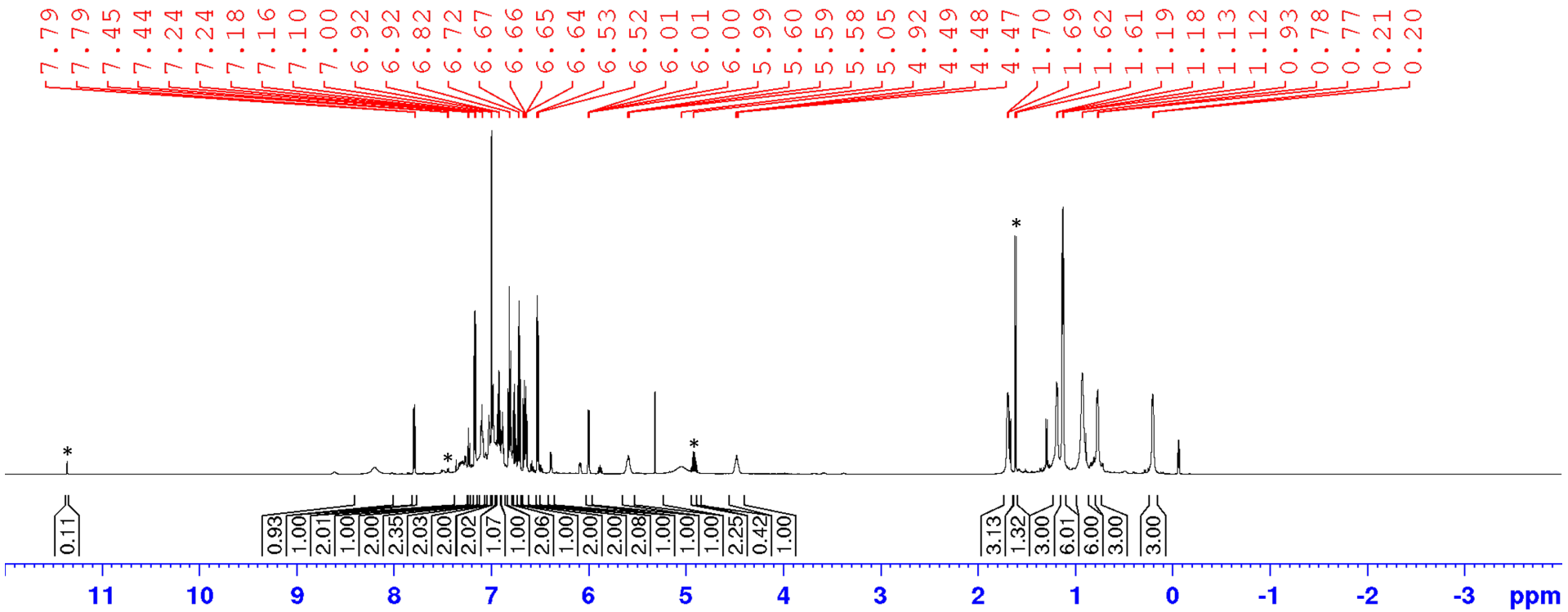

Figure S32. ^{1}H NMR spectrum of **6^{Bz}-Ph** in CD_2Cl_2. The smaller resonances marked with * are assigned to the protonated NHC, [I*i*PrH]$^{+}$, which forms alongside **6^{Bz}-Ph**.

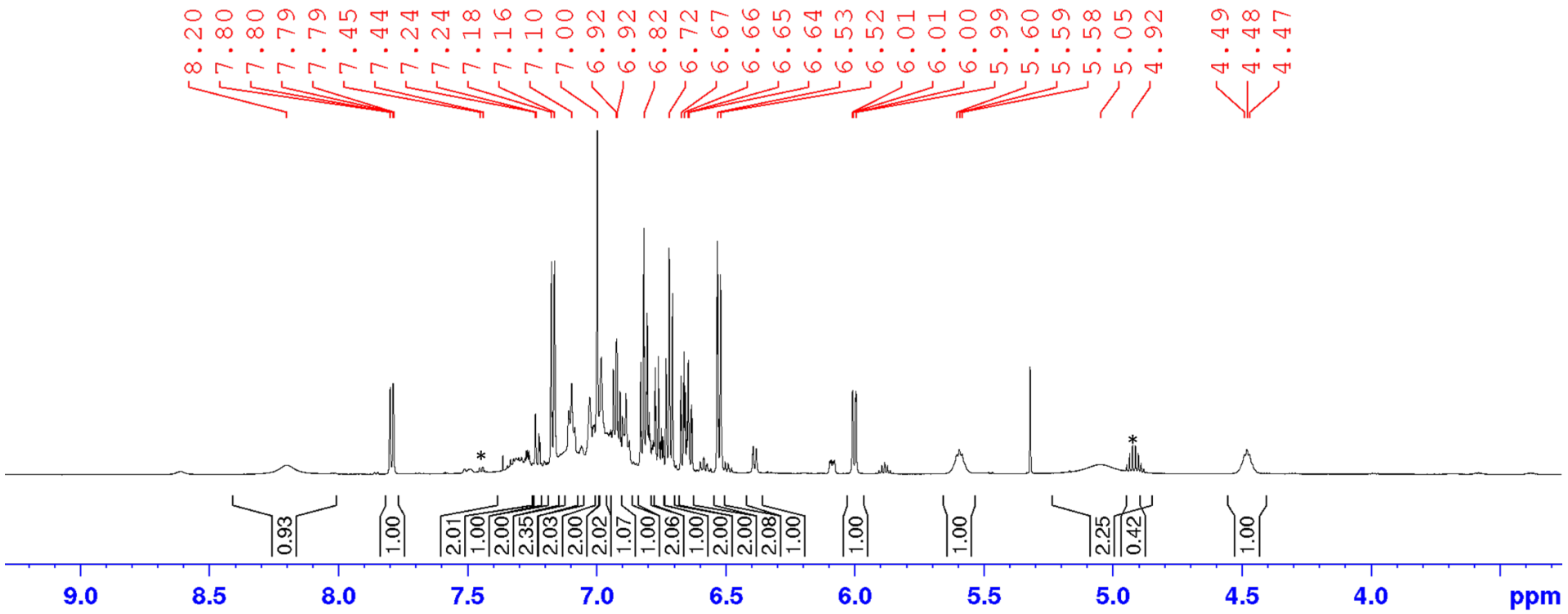

Figure S33. Expansion of the aromatic region of the ^{1}H NMR spectrum of **6^{Bz}-Ph** in CD_2Cl_2. The smaller resonances marked with * are assigned to the protonated NHC, [I*i*PrH]$^{+}$, which forms alongside **6^{Bz}-Ph**.

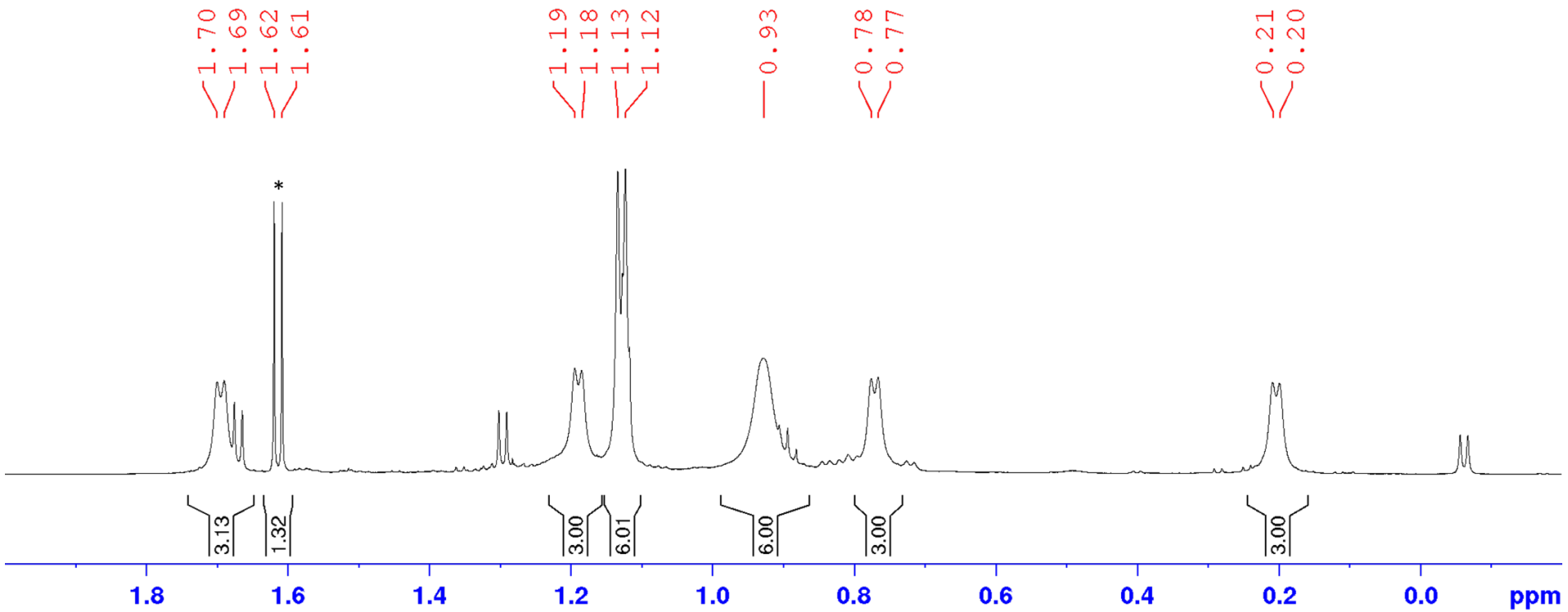

Figure S34. Expansion of the aliphatic region of the ^{1}H NMR spectrum of **6^{Bz}-Ph** in CD_2Cl_2. The smaller resonances marked with * are assigned to the protonated NHC, [I*i*PrH]$^{+}$, which forms alongside **6^{Bz}-Ph**.

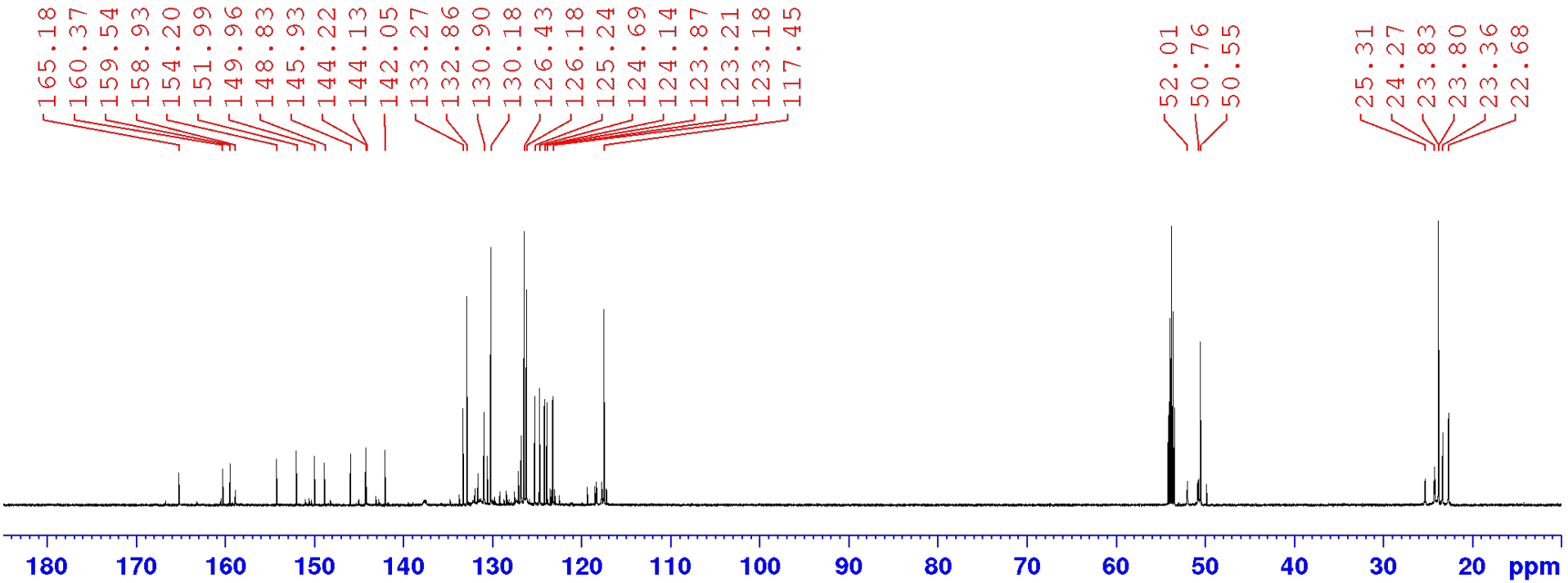

Figure S35. $^{13}C\{^{1}H, ^{11}B\}$ NMR spectrum of **6^{Bz}-Ph** in CD_2Cl_2.

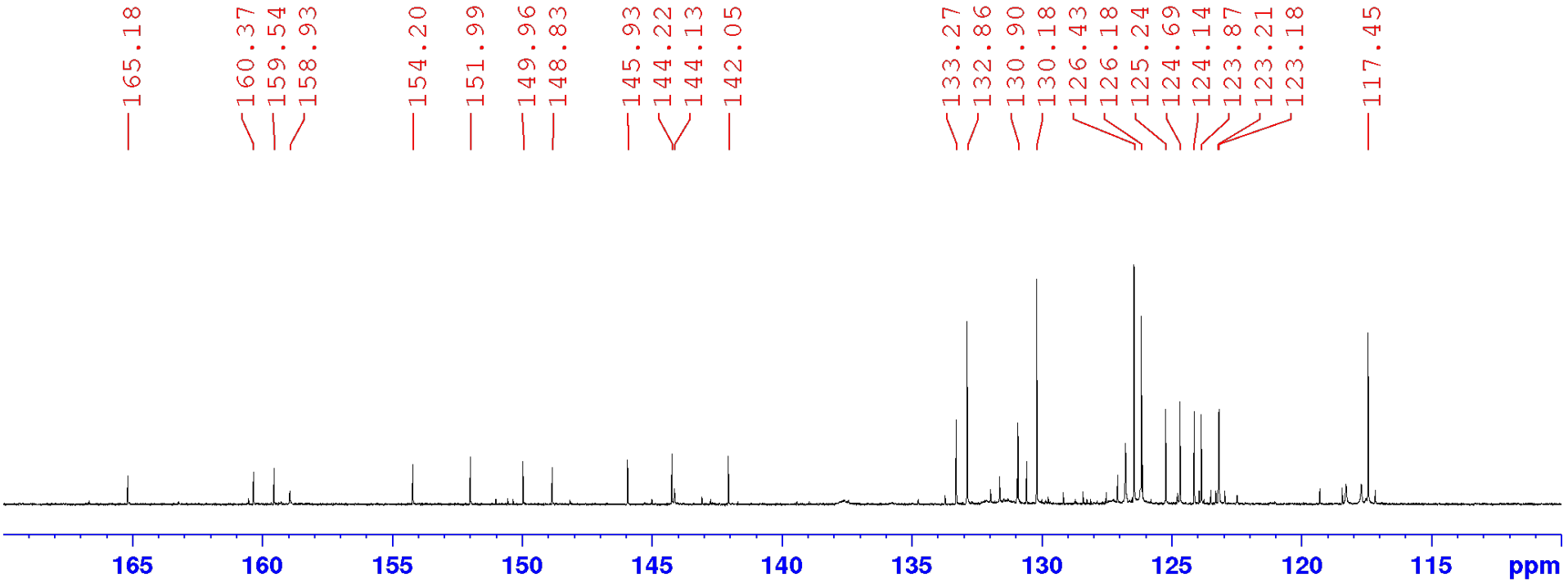

Figure S36. Expansion of the aromatic region of the $^{13}C\{^{1}H, ^{11}B\}$ NMR spectrum of **6^{Bz}-Ph** in CD_2Cl_2.

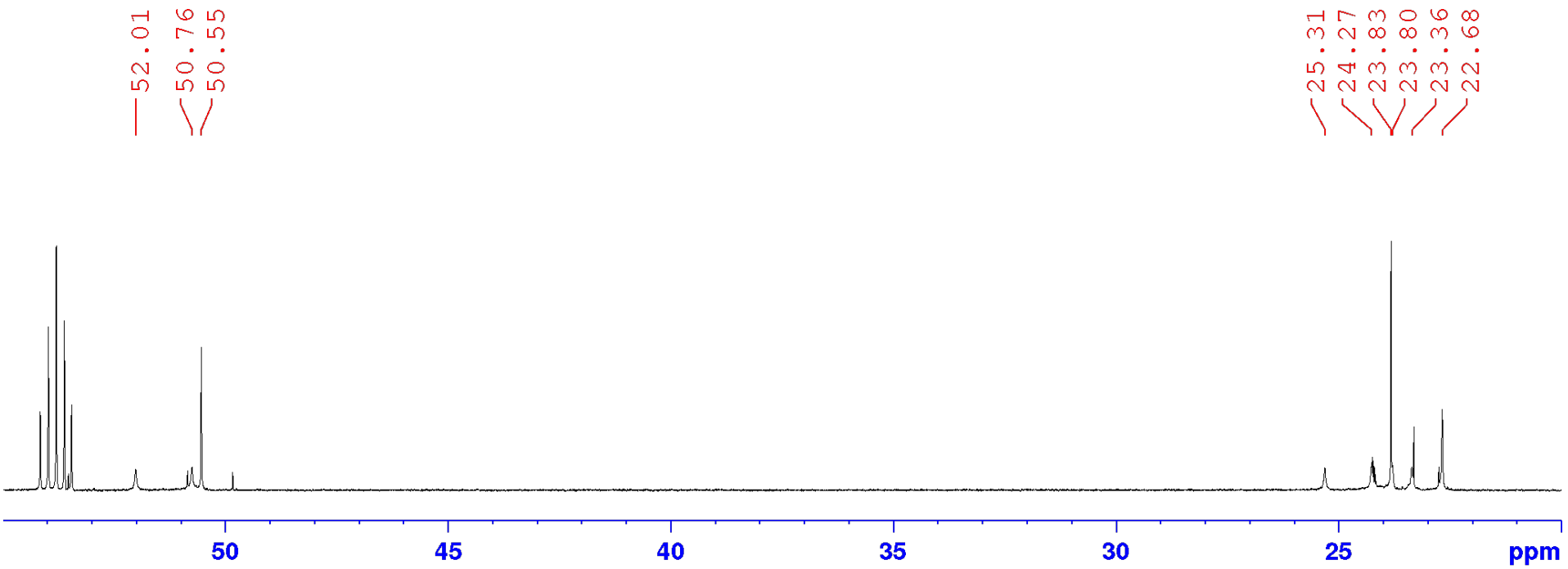

Figure S37. Expansion of the aliphatic region of the $^{13}C\{^{1}H, ^{11}B\}$ NMR spectrum of **6^{Bz}-Ph** in CD_2Cl_2.

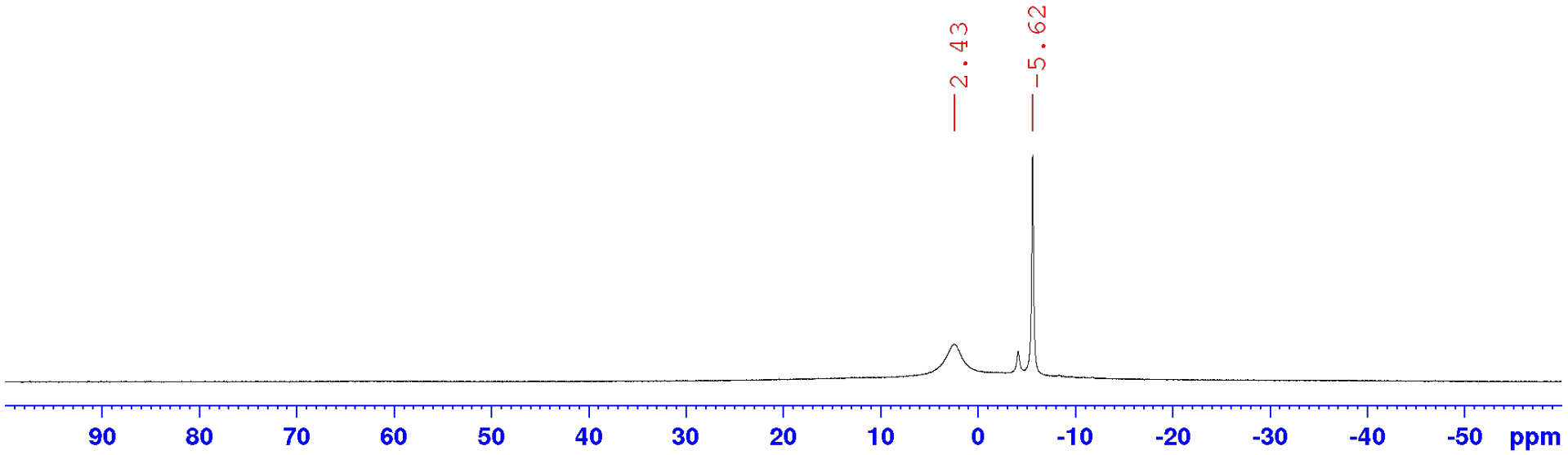

Figure S38. ^{11}B NMR spectrum of **6^{Bz}-Ph** in CD_2Cl_2 (including background reduction).

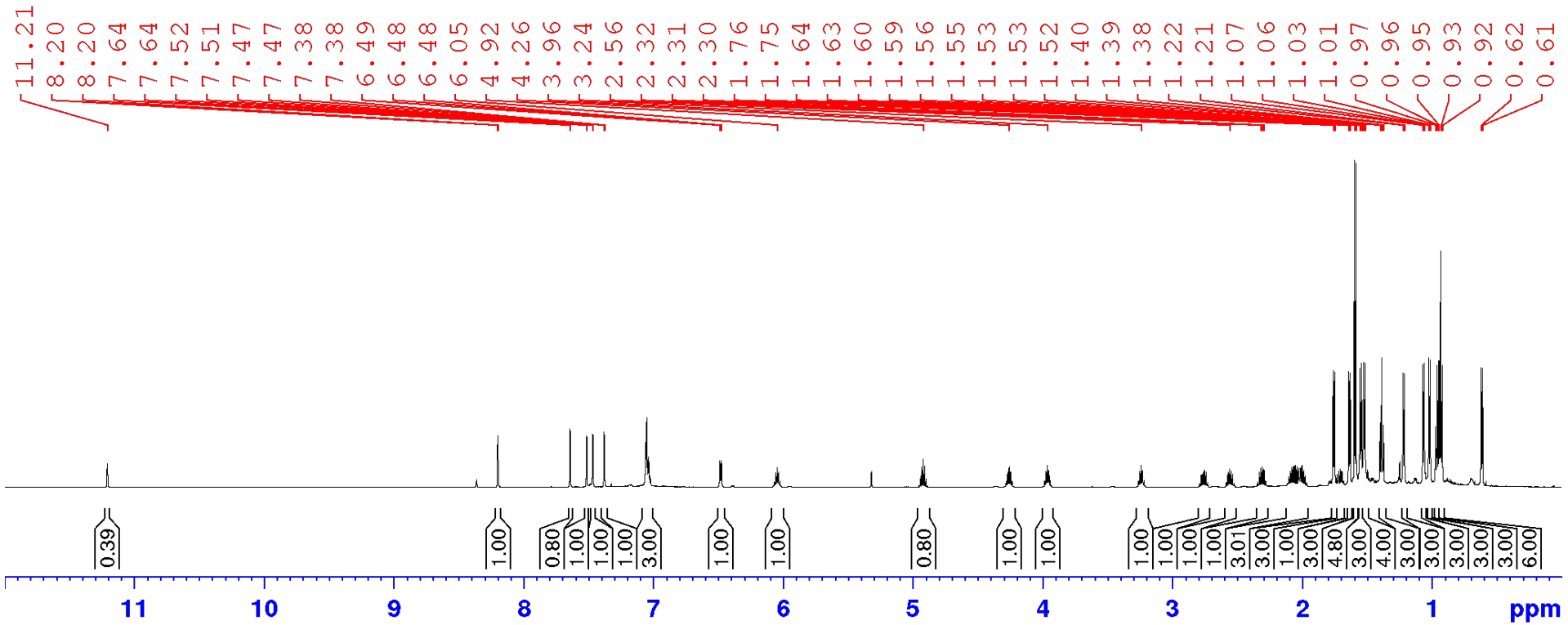

Figure S9. ^{1}H NMR spectrum of **5^{Bz}-Et** in C_6D_6.

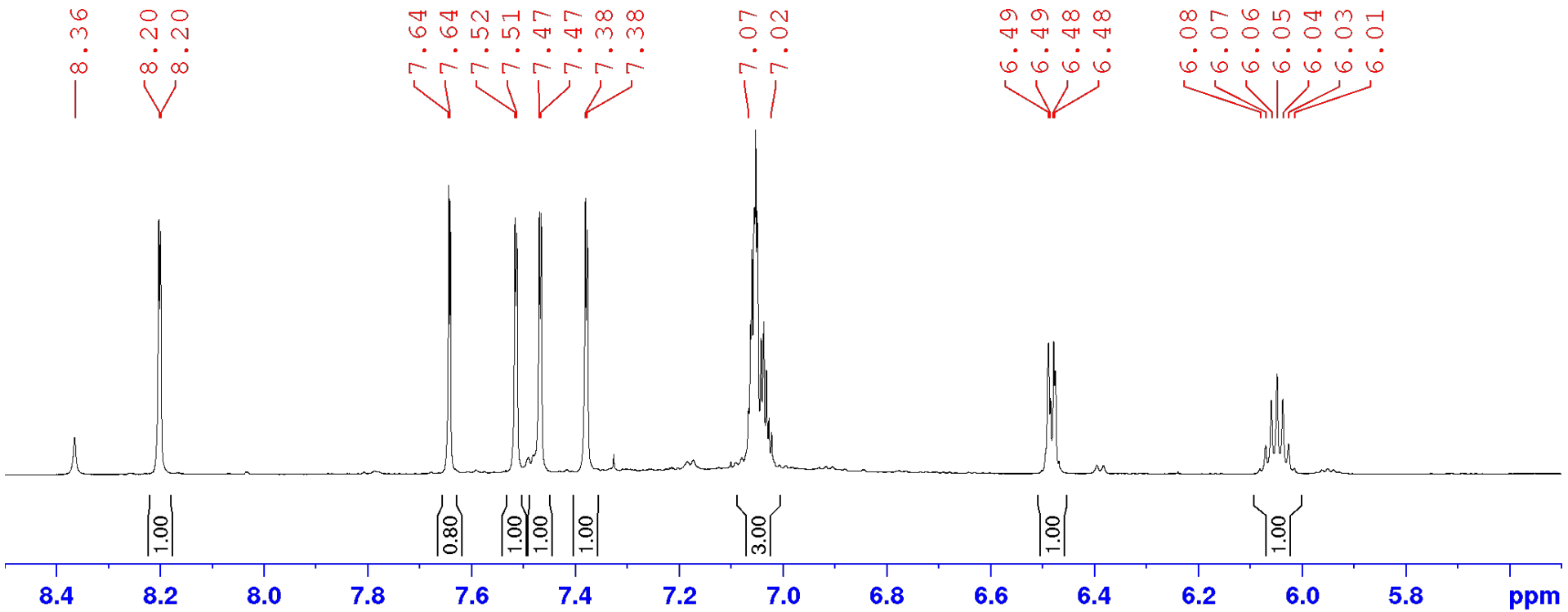

Figure S32. Expansion of the aromatic region of the ^{1}H NMR spectrum of **5^{Bz}-Et** in CD_2Cl_2.

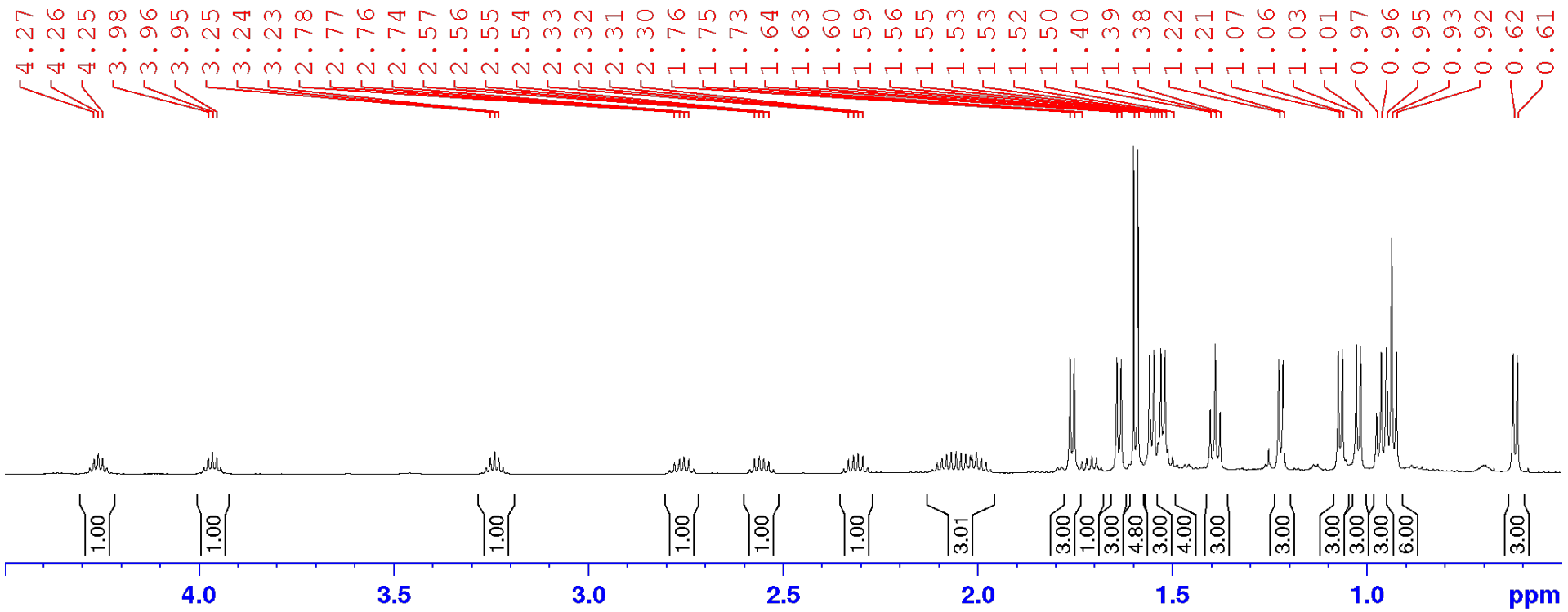

Figure S41. Expansion of the aliphatic region of the ^{1}H NMR spectrum of **5^{Bz}-Et** in CD_2Cl_2.

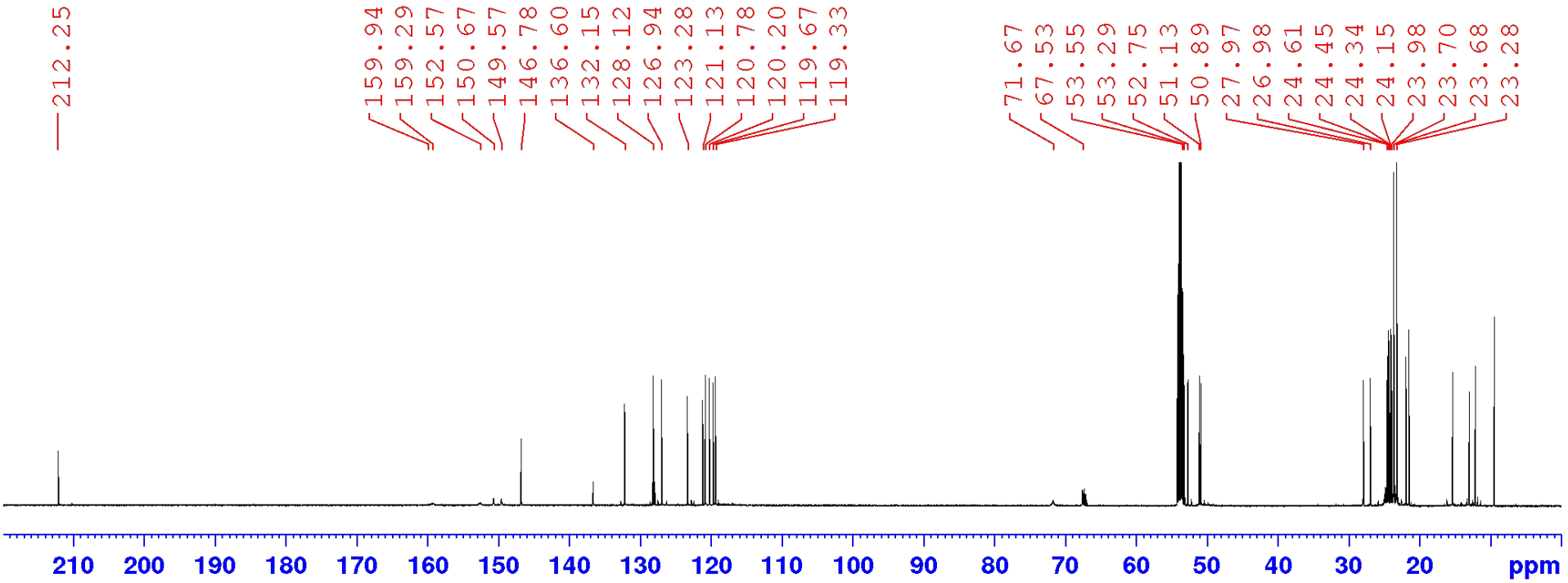

Figure S42. $^{13}C\{^{1}H\}$ NMR spectrum of **5^{Bz}-Et** in CD_2Cl_2.

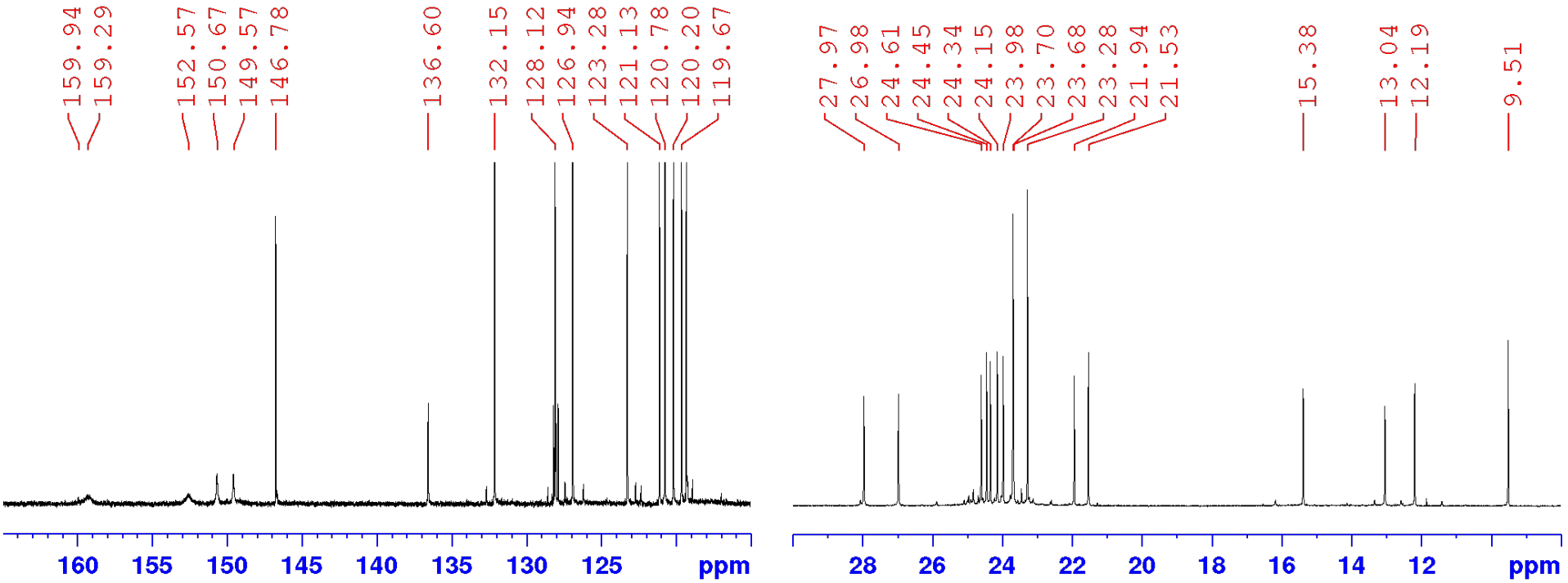

Figure S43. Expansion of the aromatic (left) and aliphatic (right) regions of the $^{13}C\{^{1}H\}$ NMR spectrum of **5^{Bz}-Et** in CD_2Cl_2.

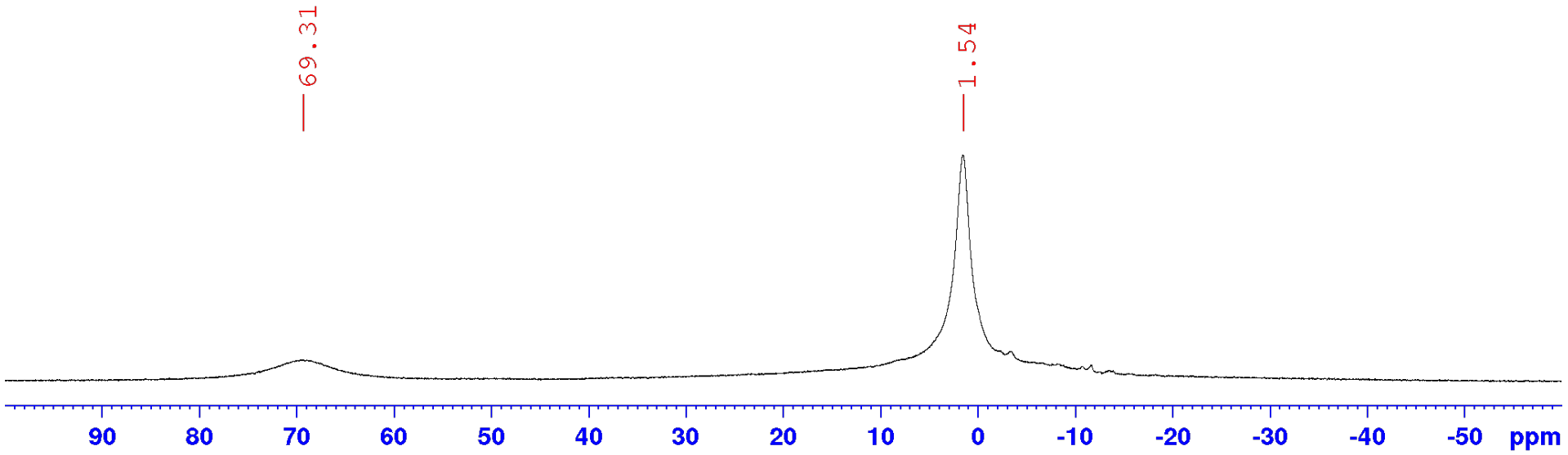

Figure S44. ^{11}B NMR spectrum of **5^{Bz}-Et** in C_6D_6 (including background reduction).

X-ray crystallographic data

The crystal data of all compounds were collected on a RIGAKU XTALAB SYNERGY-R diffractometer with a HPA area detector and multi-layer mirror monochromated $Cu_{K\alpha}$ radiation. The structure was solved using the intrinsic phasing method,[8] refined with the SHELXL program,[9] and expanded using Fourier techniques. All non-hydrogen atoms were refined anisotropically.

Crystallographic data have been deposited with the Cambridge Crystallographic Data Center as supplementary publication no. 2379410 (**3^{Bz}-Et**), 2379411 (**4^{Bz}-BzPh**), 2379412 (**3^{Bz}-Ph**), 2379413 (**6^{Bz}-Ph**), 2379414 (**3^{Bz}-BzPh**), 2379415 (**3^{Naph}-Ph**). These data can be obtained free of charge from The Cambridge Crystallographic Data Centre *via* www.ccdc.cam.ac.uk/data_request/cif.

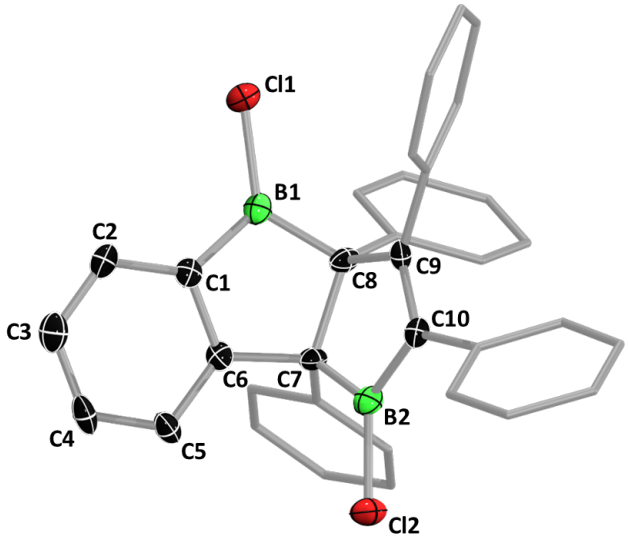

Figure S33. Solid-state structure of **3^{Bz}-Ph**. Atomic displacement ellipsoids represented at 50%. Ellipsoids of phenyl groups and hydrogen atoms omitted for clarity.

Refinement details for 3^{Bz}-Ph: The data was refined as a two-component inversion twin (BASF = 2%).

Crystal data for 3^{Bz}-Ph: $C_{34}H_{24}B_2Cl_2 \cdot C_6H_6$, $M_r = 603.16$, colourless block, 0.170×0.110×0.090 mm^3, orthorhombic space group $Pna2_1$, $a = 13.0142(3)$ Å, $b = 12.5146(4)$ Å, $c = 19.1376(7)$ Å, $V = 3116.89(17)$ Å^3, $Z = 4$, $\rho_{calcd} = 1.285$ g·cm^{-3}, $\mu = 2.076$ mm^{-1}, $F(000) = 1256$, $T = 100(2)$ K, $R_1 = 0.0714$, $wR_2 = 0.1334$, Flack parameter = 0.02(2), 5541 independent reflections [$2\theta \leq 140.14°$] and 398 parameters.

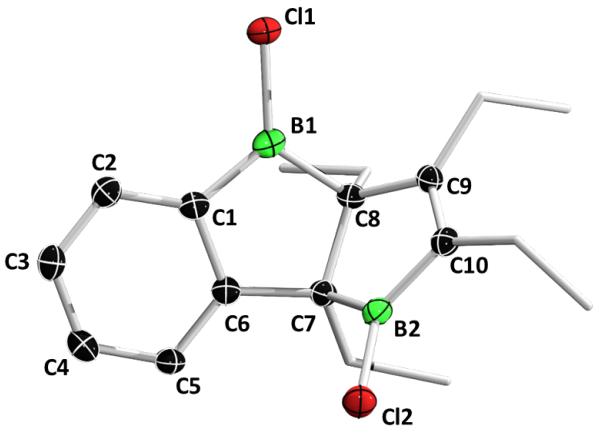

Figure S34. Solid-state structure of **3^{Bz}-Et**. Atomic displacement ellipsoids represented at 50%. Ellipsoids of ethyl groups and hydrogen atoms omitted for clarity.

Refinement details for 3^{Bz}-Et: The data was refined as a two-component inversion twin. The BASF parameter was refined to 10.3%. Two reflections were removed from refinement as outliers.

Crystal data for 3^{Bz}-Et: $C_{18}H_{24}B_2Cl_2$, M_r = 332.89, clear colourless block, 0.300×0.220×0.160 mm^3, orthorhombic space group $Pna2_1$, a = 15.1263(2) Å, b = 8.8273(2) Å, c = 26.4394(4) Å, V = 3530.31(11) Å^3, Z = 8, ρ_{calcd} = 1.253 g·cm^{-3}, μ = 3.217 mm^{-1}, $F(000)$ = 1408, T = 100(2) K, R_1 = 0.0365, wR_2 = 0.1022, Flack parameter = 0.103(16), 5833 independent reflections [$2\theta \leq 149.588°$] and 406 parameters.

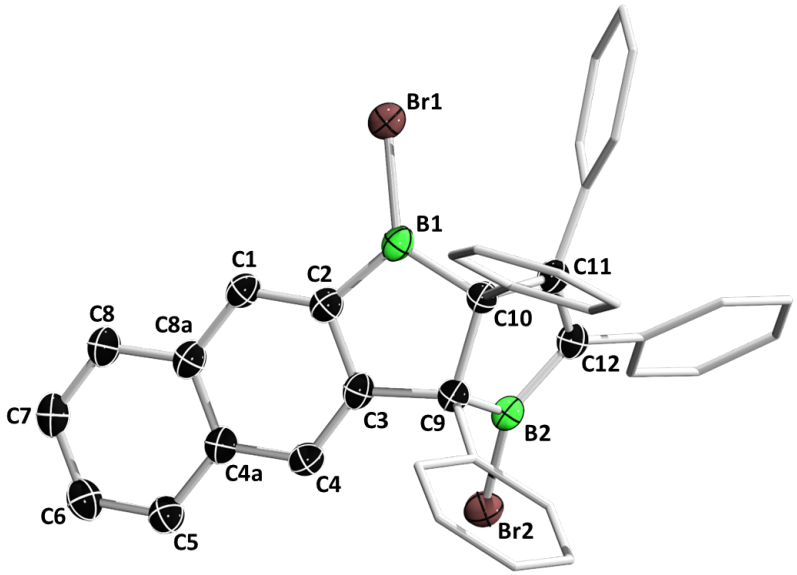

Figure S35. Solid-state structure of **3^{Naph}-Ph**. Atomic displacement ellipsoids represented at 50%. Ellipsoids of ethyl groups and hydrogen atoms omitted for clarity.

Refinement details for 3^{Naph}-Ph: Four reflections were removed from refinement as outliers.

Crystal data for 3^{Naph}-Ph: $C_{38}H_{26}B_2Br_2$, M_r = 664.03, clear light-green plate, 0.140×0.100×0.070 mm^3, monoclinic space group $P2_1/n$, a = 9.80220(10) Å, b = 8.80000(10) Å, c = 33.2868(4) Å, β = 90.3100(10)°, V = 2871.26(6) Å^3, Z = 4, ρ_{calcd} = 1.536 g·cm^{-3}, μ = 3.778 mm^{-1}, $F(000)$ = 1336, T = 100(2) K, R_1 = 0.0475, wR_2 = 0.1277, 5714 independent reflections [$2\theta \leq 149.88°$] and 379 parameters.

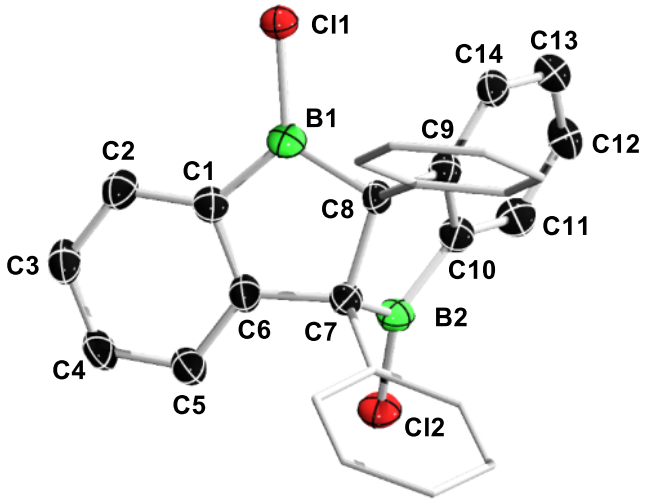

Figure S36. Solid-state structure of **3^{Bz}-BzPh**. Atomic displacement ellipsoids represented at 50%. Ellipsoids of phenyl groups and hydrogen atoms omitted for clarity.

Refinement details for 3^{Bz}-BzPh: Two reflections were removed from refinement as outliers (-1 12 8, -1 11 9).

Crystal data for 3^{Bz}-BzPh: $C_{26}H_{18}B_2Cl_2$, $M_r = 422.92$, colourless block, 0.220×0.070×0.040 mm^3, triclinic space group $P\bar{1}$, $a = 8.5722(3)$ Å, $b = 12.2762(4)$ Å, $c = 21.3971(5)$ Å, $\alpha = 95.172(2)°$, $\beta = 93.665(2)°$, $\gamma = 109.945(3)°$, $V = 2097.22(12)$ Å^3, $Z = 4$, $\rho_{calcd} = 1.339$ g·cm^{-3}, $\mu = 2.844$ mm^{-1}, $F(000) = 872$, $T = 100(2)$ K, $R_1 = 0.0809$, $wR_2 = 0.2151$, 7613 independent reflections [$2\theta \leq 136.494°$] and 541 parameters.

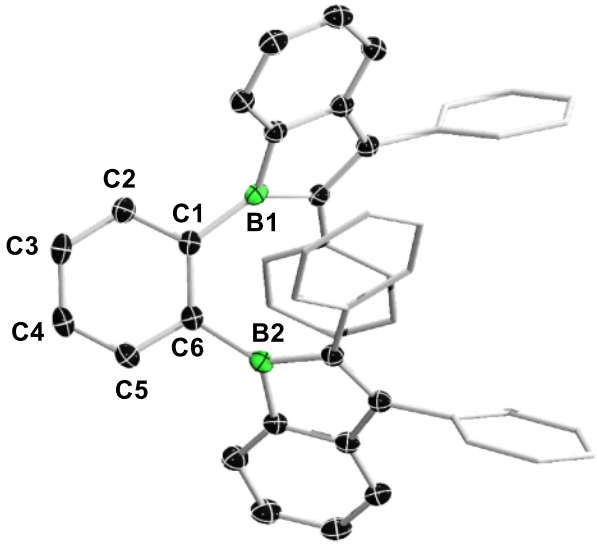

Figure S37. Solid-state structure of **4^{Bz}-BzPh**. Atomic displacement ellipsoids represented at 50%. Ellipsoids of phenyl groups and hydrogen atoms omitted for clarity.

Refinement details for 4^{Bz}-BzPh: The asymmetric unit contains one benzene molecule modelled as twofold rotationally disordered (RESI 61 and 62 SOLV) in a 54:46 ratio. The benzene rings within the disorder were idealised with AFIX 66 and ADPs restrained with SIMU 0.01.

Crystal data for 4^{Bz}-BzPh: $C_{46}H_{32}B_2 \cdot C_6H_6$, $M_r = 684.44$, clear dark-red block, 0.270×0.200×0.110 mm^3, orthorhombic space group *Pbca*, $a = 20.95130(10)$ Å, $b = 15.16980(10)$ Å, $c = 23.25820(10)$ Å, $V = 7392.08(7)$ Å^3, $Z = 8$, $\rho_{calcd} = 1.230$ g·cm^{-3}, $\mu = 0.518$ mm^{-1}, $F(000) = 2880$, $T = 100(2)$ K, $R_1 = 0.0408$, $wR_2 = 0.0905$, 7542 independent reflections [$2\theta \leq 149.972°$] and 518 parameters.

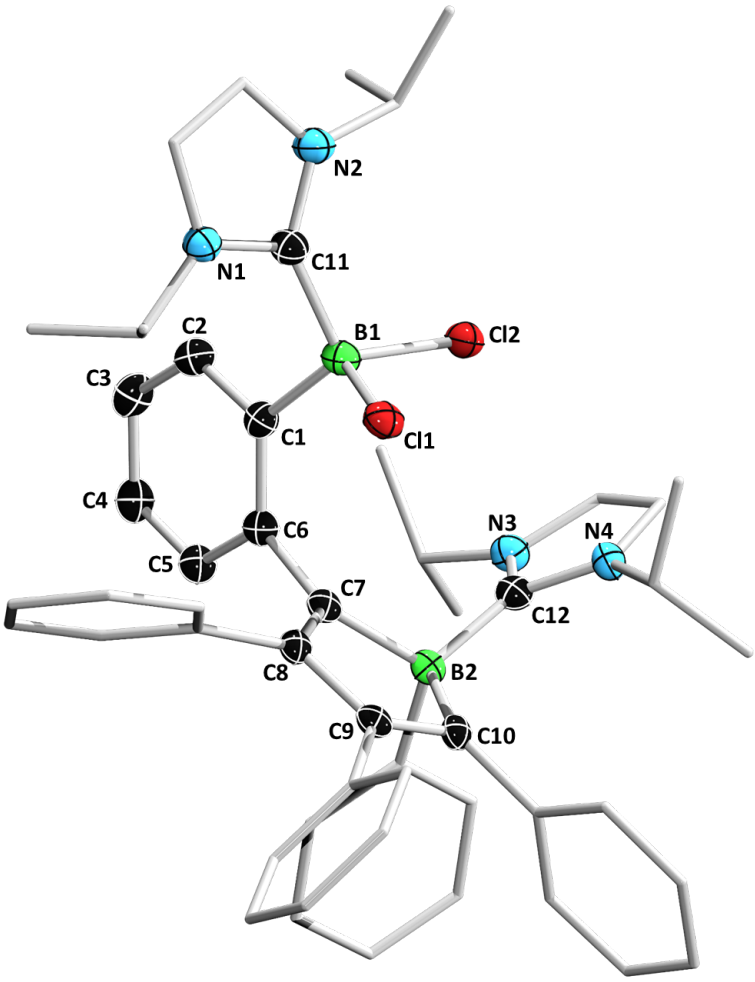

Figure S38. Solid-state structure of **6^{Bz}-Ph**. Atomic displacement ellipsoids represented at 50%. Ellipsoids of ethyl groups and hydrogen atoms omitted for clarity.

Refinement details for 6^{Bz}-Ph: Two reflections (14 -4 8, 15 -4 5) were removed from refinement as outliers. A highly disordered DCM molecule positioned an inversion centre was treated as a diffuse contribution to the overall scattering without specific atom positions by SQUEEZE/PLATON.[10] 41 electrons were thus removed from the unit cell, corresponding to ca. one DCM molecule.

Crystal data for 6^{Bz}-Ph: $C_{52}H_{56}B_2Cl_2N_4 \cdot (CH_2Cl_2)[\cdot(CH_2Cl_2)_{0.5}]_{squeezed}$, $M_r = 956.91$, clear light-yellow plate, 0.150×0.110×0.070 mm^3, triclinic space group $P\bar{1}$, $a = 12.6381(3)$ Å, $b = 12.7947(3)$ Å, $c = 15.9160(2)$ Å, $\alpha = 98.8360(10)°$, $\beta = 91.4760(10)°$, $\gamma = 98.891(2)°$, $V = 2509.29(9)$ Å^3, $Z = 2$, $\rho_{calcd} = 1.266$ g·cm^{-3}, $\mu = 2.935$ mm^{-1}, $F(000) = 1006$, $T = 100(2)$ K, $R_1 = 0.0578$, $wR_2 = 0.1277$, 9719 independent reflections [$2\theta \leq 149.826°$] and 660 parameters.

Computational details

All density functional theory (DFT) optimisations were carried out at the B3LYP[11]-D3(BJ)[12]-def2-SVP[13] level of theory using the Turbomole (version 7.6)[14] user interface TmoleX2022.[15] True minima were confirmed by frequency calculations, which provided no imaginary frequencies. Transition states guesses (TS_{guess}) were preoptimized at the B3LYP-D3(BJ)-def-SV(P) level of theory by fixing only the atoms relevant to the transformation in the estimated transition state position and allowing the rest of the molecules to optimize freely. IR and lowest Hessian eigenvalue calculations were carried out on TS_{guess} to determine which imaginary frequency corresponds to the vibrational mode relevant to the desired transformation, as visualized in the TmoleX2022 Vibrations viewer. The TS was then freely optimized following the corresponding eigenvector and recalculating the Hessian every five optimization steps. True TS maxima were confirmed by full IR calculations, which provided a single imaginary frequency, which was confirmed as transformation-relevant by visualization of the corresponding vibrational mode in the TmoleX2022 Vibrations viewer.

To benchmark the level of theory best suited to calculating the Gibbs free energies for the mechanism, the energies of **Int1**, **TS1** and **Int2** were computed at the coupled-cluster approximate singles and doubles (CC2)[16] method (freezing the lowest energy 46 MOs) using the def2-SVP (auxiliary) basis sets, in combination with the resolution of identity approximation for coulomb integrals (RI)[17] and the numerical chain-of-spheres integration for the Hartree-Fock exchange integrals (COS).[18] This method was chosen as it is computationally relatively efficient, while still delivering similar results to the more accurate coupled-cluster singles and doubles method CCSD, which has proven reliable for computing accurate reaction mechanisms and barriers.[19] The MP2[20] method and the DFT-B3LYP level of theory overestimate the reaction barrier and reaction energy, whereas the TPSS[21] level of theory underestimates both. The PBE0 level of theory,[22] which has also proven itself to provide reliable mechanistic data,[19b,23] was found to overestimate both reaction barrier and energy the least. Consequently, higher-level Gibbs free energies at 298 K were calculated at the PBE0-D3(BJ)-def2-mTZVPP[23] level of theory, using the solvent correction method COSMO(benzene)[25] on the optimized structures using the following equation:

$$G_{298K} = (E_{COSMO} + C_{solv})_{higher\ level} + (CP_{298K})_{lower\_level}$$

Where E_{COSMO} = SCF energy of the PBE0-D3(BJ)-def2-mTZVPP-COSMO(C_6H_6) calculation

C_{solv} = Solvent correction (= dielectric energy + outlying charge correction) of the PBE0-D3(BJ)-def2-mTZVPP-COSMO(C_6H_6) calculation

CP_{298K} = chemical potential at 298 K of the B3LYP-D3(BJ)-def2-SVP optimisation

The Cartesian coordinates of all optimised intermediates and transition states are provided in a separate Coordinates_of_optimised_structures.xyz file.

Table S1. SCF energies (E, Ha) computed for the optimised (B3LYP-D3(BJ)-def2-SVP) structures of **Int1**, **TS1** and **Int2**, as well as activation energies ($\Delta E_{1\text{-}2}^{\ddagger}$, kcal mol^{-1}) and reaction energies ($\Delta E_{1\text{-}2}$, kcal mol^{-1}) for the step **Int1→Int2**, calculated at various levels of theory for benchmarking purposes.

	E_{Int1} (Ha)	E_{TS1} (Ha)	E_{Int2} (Ha)	$\Delta E_{1\text{-}2}^{\ddagger}$ (kcal mol^{-1})	$\Delta E_{1\text{-}2}$ (kcal mol^{-1})
CC2/MP2(SOS)-def2-SVP	-2273.5748	-2273.5617	-2273.5673	8.20	4.74
MP2-def2-SVP	-2273.5177	-2273.4966	-2273.5007	13.21	10.63
B3LYP-D3(BJ)-def2-SVP	-2278.2012	-2278.1800	-2278.1866	13.31	9.14
CAM-B3LYP-D3(BJ)-def2-SVP	-2278.3119	-2278.2864	-2278.2925	16.01	12.21
PBE0-D3(BJ)-def2-SVP	-2277.1935	-2277.1774	-2277.1853	10.10	5.13
TPSS-D3(BJ)-def2-SVP	-2279.4664	-2279.4544	-2279.4627	7.55	2.33

It is noteworthy that the energy barriers of the reaction profile are highly sensitive to the direction of the propeller-like arrangement of the four phenyl substituents. Great care has to be taken to work backwards from the product **3^{Bz}-Ph** and maintain the correct orientation of the phenyl substituents throughout the entire reaction pathway, as these are prone to rotation during optimization, which then leads to higher reaction barriers. For the RDS, in particular, the overall SCF energy barrier from the axial isomer **Int1-a** to **TS3-a** is 7.5 kcal mol^{-1} lower than from **Int1-b** (Figure S38).

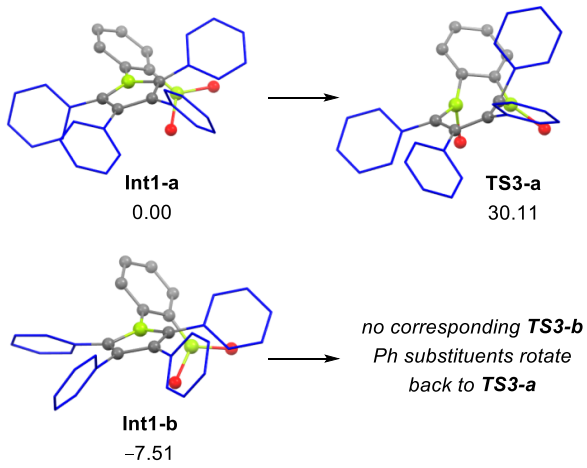

Figure S39. Optimised structures of the species relevant to the RDS with two different propeller arrangements (a and b) of the phenyl groups. SCF in kcal mol^{-1}.

For the rearrangement of **Int2** to **Int4** two pathways were considered (Figure S40):

- Cl transfer from one boron to the other to yield **Int3**, followed by B−C bond cleavage (in green), with an overall barrier of 29.4 kcal mol^{-1} from **Int1**.
- B−C bond cleavage to yield **Int3'**, followed by Cl transfer from one boron to the other (in orange), with an overall barrier of 26.9 kcal mol^{-1} from **Int1**.

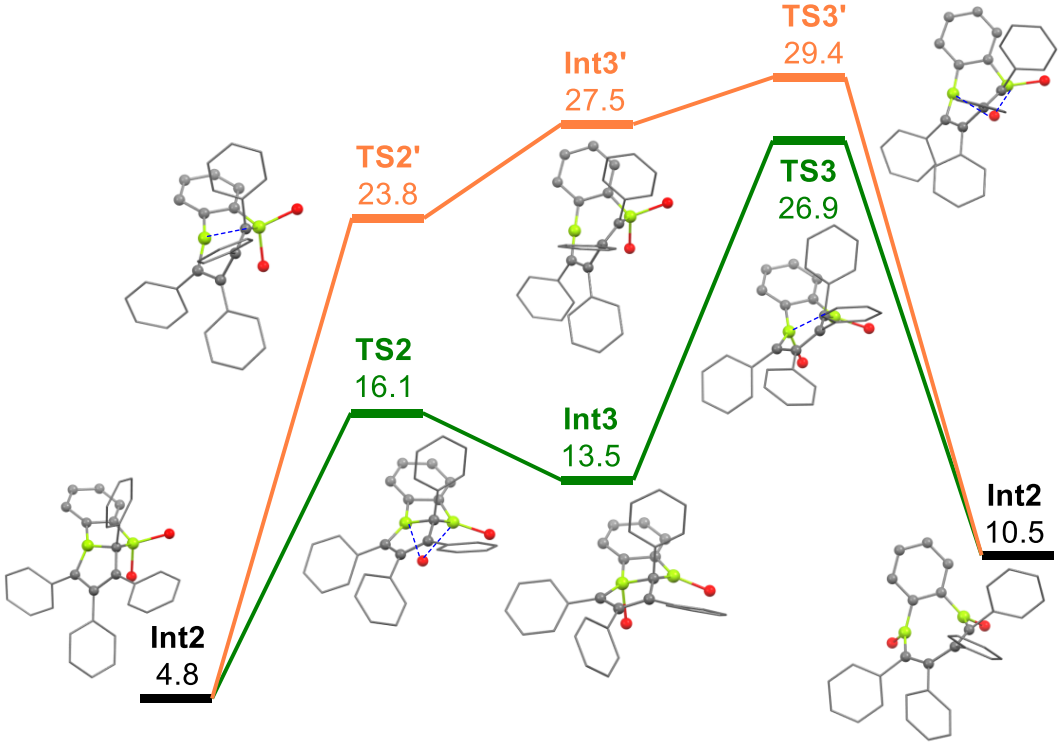

Figure S40. Alternative mechanisms for the rearrangement of **Int2** to **Int4** in benzene at 25 °C. Gibbs free energies (kcal mol^{-1}) computed at the COSMO(C_6H_6)-PBE0-D3(BJ)-Def2-mTZVPP//B3LYP-D3(BJ)-Def2-SVP level of theory.

Table S2. Lowest frequencies (ν_{min}), SCF energies (E_{SCF}), relative SCF energies versus **Int1** (ΔE_{SCF}), zero-point vibrational energy-corrected SCF energies (E_0) and chemical potential at 298 K (CP_{298}) calculated at the B3LYP-D3(BJ)-Def2-SVP level of theory. SCF energy and solvent correction (E_{COSMO} and C_{solv}) calculated at the PBE0-D3(BJ)-Def2-mTZVPP-COSMO(C_6H_6) level of theory, solvent-corrected Gibbs free energy at 298 K (ΔG_{298}), and relative Gibbs free energy versus **Int** at 298 K (ΔG_{298}).

	ν_{min} (cm^{-1})	E_{SCf} (Ha)	ΔE_{SCF} (kcal mol^{-1})	E_0 (Ha)	CP_{298} (Ha)	E_{COSMO} (Ha)	C_{solv} (Ha)	G_{298} (Ha)	ΔG_{298} (kcal mol^{-1})
Int1	5.04	-2278.2012	0.00	-2277.7199	0.4133	-2278.8743	-0.00915	-2278.47016	0.00
TS1	-201.00	-2278.1800	13.31	-2277.6998	0.4160	-2278.8594	-0.01169	-2278.45514	9.43
Int2	21.40	-2278.1866	9.14	-2277.7050	0.4180	-2278.8681	-0.01236	-2278.46244	4.84
TS2	-122.95	-2278.1684	20.58	-2277.6875	0.4177	-2278.8505	-0.01165	-2278.44445	16.14
Int3	16.26	-2278.1719	18.39	-2277.6905	0.4167	-2278.8539	-0.01138	-2278.44863	13.51
TS3	-216.45	-2278.1532	30.11	-2277.6739	0.4152	-2278.8324	-0.01022	-2278.42736	26.86
TS2'	-124.8	-2278.1512	38.87	-2277.6716	0.4151	-2278.8339	-0.01348	-2278.43220	23.82
Int2'	14.03	-2278.1505	39.35	-2277.6707	0.4141	-2278.8268	-0.01365	-2278.42629	27.53
TS3'	-96.9	-2278.1499	39.71	-2277.6703	0.4152	-2278.8263	-0.01220	-2278.42332	29.39
Int4	9.34	-2278.1837	10.96	-2277.7034	0.4134	-2278.8574	-0.00941	-2278.45339	10.52
Int5	19.34	-2278.2245	-14.64	-2277.7430	0.4155	-2278.8992	-0.00885	-2278.49262	-14.09
TS5	-128.88	-2278.2159	-9.21	-2277.7349	0.4177	-2278.8954	-0.00969	-2278.48741	-10.82
Int6	22.49	-2278.2164	-9.54	-2277.7345	0.4180	-2278.8968	-0.01011	-2278.48889	-11.75
TS6	-378.40	-2278.1875	8.58	-2277.7063	0.4185	-2278.8689	-0.00900	-2278.45940	6.75
Int7	21.49	-2278.2245	-14.63	-2277.7410	0.4208	-2278.9061	-0.00804	-2278.49340	-14.58
TS7	-186.81	-2278.2003	0.55	-2277.7185	0.4194	-2278.8887	-0.00839	-2278.47774	-4.76
3^{Bz}–Ph	23.36	-2278.2401	-24.42	-2277.7568	0.4204	-2278.9209	-0.00810	-2278.50865	-24.15

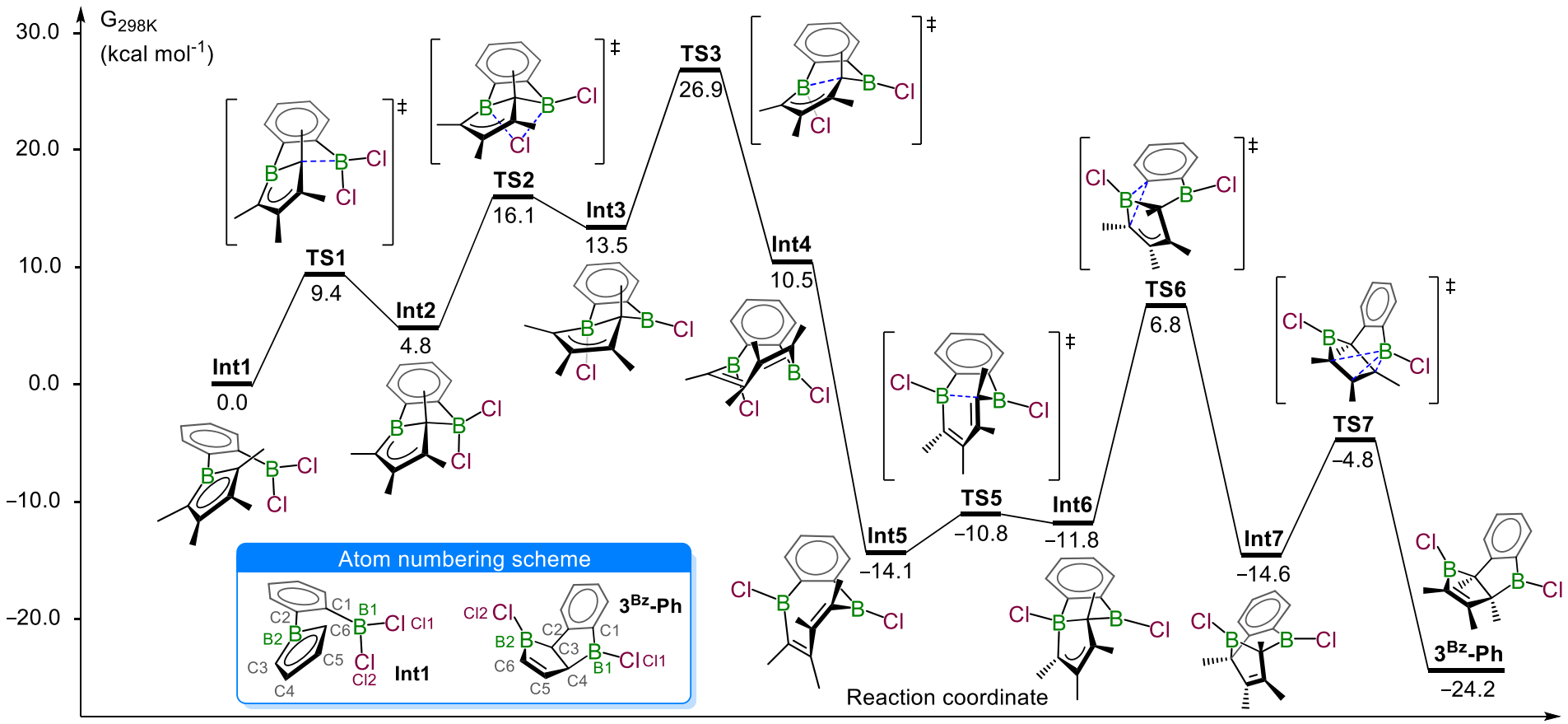

Figure S41. Calculated lowest-energy mechanism for the formation of **3^{Bz}-Ph** (phenyl substituents omitted for clarity) in benzene at 25 °C. Gibbs free energies (kcal mol^{-1}) computed at the COSMO(C_6H_6)-PBE0-D3(BJ)-Def2-mTZVPP//B3LYP-D3(BJ)-Def2-SVP level of theory.

References

1. D. Kaufmann, *Chem. Ber.*, 1987, **120**, 901−905.
2. A. Gärtner, L. Meier, M. Arrowsmith, M. Dietz, I. Krummenacher, R. Bertermann, F. Fantuzzi and H. Braunschweig, *J. Am. Chem. Soc.*, 2022, **144**, 21363–21370.
3. (a) F. C. Leavitt, T. A. Manuel and F. Johnson, *J. Am. Chem. Soc.*, 1959, **81**, 3163–3164; (b) F. C. Leavitt, T. A. Manuel, F. Johnson, L. U. Matternas and D. S. Lehman, *J. Am. Chem. Soc.*, 1960, **82**, 5099−5102.
4. (a) Y. Ura, Y. Li, Z. Xi and T. Takahashi, *Tetrahedron Lett.*, 1998, **39**, 2787−2790; (b) J. L. Bohlen, L. Endres, R. Drescher, K. Radacki, M. Dietz, I. Krummenacher and H. Braunschweig, *Chem. Sci.*, 2023, **14**, 9010−9015.
5. S.-B. Choi, P. Boudjouk and K. Qin, *Organometallics*, 2000, **19**, 1806−1809.
6. M. Niehues, G. Kehr, G. Erker, B. Wibbeling, R. Fröhlich, O. Blacque and H. Behr, *J. Organomet. Chem.*, 2002, 192−203.
7. A. Y. Houghton, Doctoral thesis: *On the Syntheses and Reactions of Boroles and Boraindenes*, University of Calgary, 2014.
8. G. Sheldrick, *Acta Cryst.*, 2015, **A71**, 3−8.
9. G. Sheldrick, *Acta Cryst.*, 2008, **A64**, 112−122.
10. A. L. Spek, *Acta Cryst.*, 2015, **C71**, 9–18.
11. (a) A. D. Becke, *J. Chem. Phys*., 1993, **98**, 5648–5652; (b) C. Lee, W. Yang and R. G. Parr, *Phys. Rev. B*, 1988, **37b**, 785–789; (c) S. H. Vosko, L. Wilk and M. Nusair, *Can. J. Phys*., 1980, **58**, 1200–1211; (d) P. J. Stephens, F. J. Devlin, C. F. Chabalowski and M. J. Frisch, *J. Phys. Chem.*, 1994, **98**, 11623–11627.
12. S. Grimme, S. Ehrlich and L. Goerigk, *J. Comput. Chem*., 2011, **32**, 1456–1465.
13. (a) F. Weigend and R. Ahlrichs, *Phys. Chem. Chem. Phys.*, 2005, **7**, 3297–3305; (b) F. Weigend, *Phys. Chem. Chem. Phys*., 2006, **8**, 1057–1065.
14. TURBOMOLE V7.6, a development of University of Karlsruhe, Forschungszentrum Karlsruhe GmbH, 1989–2007; TURBOMOLE GmbH, since 2007; available from http://www.turbomole.com.TmoleX2022.
15. TmoleX2022, Dassault Systèmes, Versailles.
16. (a) O. Christiansen, H. Koch and P. Jørgensen, *Chem. Phys. Lett.*, 1995, **243**, 409–418; (b) S. D. Folkestad and H. Koch, *Chem. Theory Comput.*, 2020, **16**, 179–189.
17. K. Eichkorn, O. Treutler, H. Öhm, M. Häser and R. Ahlrichs. *Chem. Phys. Lett.*, 1995, **240**, 283–290.

18. F. Neese, F. Wennmohs, A. Hansen and U. Becker, *Chem. Phys.*, 2009, **356**, 98–109.
19. (a) R. J. Bartlett and M. Musiał, *Rev. Mod. Phys.*, 2007, **79**, 291–352; (b) T. Piskor, P. Pinski, T. Mast and V. Rybkin, *Int. J. Mol. Sci*., 2024, **25**, 8530; (c) G. D. Purvis and R. J. Bartlett, *J. Chem. Phys*., 1982, **76**, 1910–1918.
20. (a) M. J. Frisch, M. Head-Gordon and J. A. Pople, *Chem. Phys. Lett.*, 1990, **166**, 275–280; (b) M. J. Frisch, M. Head-Gordon and J. A. Pople, *Chem. Phys. Lett.*, 1990, **166**, 281–289.
21. J. Tao, J. P. Perdew, V. N. Staroverov and G. E. Scuseria, *Phys. Rev. Lett*., 2003, **91**, 146401.
22. (a) C. Adamo and V. Barone, *J. Chem. Phys.*, 1999, **110**, 6158–6170; (b) J. P. Perdew, K. Burke and M. Ernzerhof, *Phys. Rev. Lett.*,1996, **77**, 3865.
23. (a) W. Wang, Y. Zhang and Y.-B. Wang, *Int. J. Quantum Chem*., 2017, **117**, e25345; (b) S. Gurtu, S. Rai, M. Ehara and U. D. Priyakumar, *Theor. Chem. Acc*., 2016, **135**, 93; (c) W. M. C. Sameera and D. A. Pantazis, *J. Chem. Theory Comput.*, 2012, **8**, 2630–2645; (d) G. I. Csonka and J. Kaminsky, *J. Chem. Theory Comput.*, 2011, **7**, 988–997.
24. S. Grimme, A. Hansen, S. Ehlert and J.-M. Mewes, *J. Chem. Phys*., 2021, **154**, 064103.
25. A. Klamt and G. Schüürmann, *J. Chem. Soc. Perkin Trans*., 1993, **2**, 799–805.